The International Journal of Advanced Manufacturing Technology (2022) 120:103–135
https://doi.org/10.1007/s00170-022-08731-1

CRITICAL REVIEW

Micro-texturing of polymer surfaces using lasers: a review

Amarachi F. Obilor[1,2] · Manuela Pacella[1] · Andy Wilson[3] · Vadim V. Silberschmidt[1]

Received: 30 July 2021 / Accepted: 12 January 2022 / Published online: 11 February 2022

Abstract

Micro- and nanoscale structures produced on surfaces of metals, polymers, ceramics, and glasses have many important applications in different fields such as engineering, medical, biological, etc. Laser ablation using ultrashort pulses has become the prominent technique for generating different surface structures for various functional applications. Ultrashort laser ablation proved to be ideal for producing structures with dimensions down to the nanometre scale. In comparison to other texturing techniques employed to create micro/nano features such as electrochemical machining, micro-milling, ion-beam etching, hot embossing, lithography, and mechanical texturing, ultrashort laser ablation produces high-quality surfaces at low cost in a one-step non-contact process. Advantageous characteristics of polymers such as high strength-to-weight ratio, non-corrosive nature, and high electrical and thermal resistance, have made polymers the preferred choice compared to other materials (e.g., steel, aluminium, titanium) in several fields of application. As a result, laser ablation of polymers has been of great interest for many researchers. This paper reviews the current state-of-the art research and recent progress in laser ablation of polymers starting from laser-material interaction, polymer properties influenced by laser, laser texturing methods, and achievable surface functionalities such as adhesion, friction, self-cleaning, and hydrophilicity on commonly used polymeric materials. It also highlights the capabilities and drawbacks of various micro-texturing techniques while identifying texture geometries that can be generated with these techniques. In general, the objective of this work is to present a thorough review on laser ablation and laser surface modification of a variety of industrially used polymers. Since direct laser interference patterning is an emerging area, considerable attention is given to this technique with the aim of forming a basis for follow-up research that could pave the way for potential technological ideas and optimization towards obtaining complex high-resolution features for future novel applications.

Keywords Polymer · Laser surface modification · Surface texturing · Wettability · Adhesion · Direct laser writing · Direct laser interference patterning

Acronyms

Arf	Argon fluoride
CA	Contact angle
DLIP	Direct laser interference patterning
DLW	Direct laser writing
HDPE	High-density polyethylene
IR	Infrared
LDPE	Low-density polyethylene
LST	Laser surface texturing
NR	Natural rubber
PC	Polycarbonate
PDMS	Polydimethylsilixane
PE	Polyethylene
PEEK	Polyetheretherketone
PES	Polyester
PET	Polyethylene terephthalate
PF	Phenol formaldehyde resin
PI	Polyimide
PLA	Polylactic acid
PMMA	Polymethylmethacrylate
POM	Polyoxymethylene
PP	Polypropylene
PS	Polystyrene
PSU	Polysulfone
PTFE	Polytetrafluoroethylene

✉ Manuela Pacella
M.Pacella@lboro.ac.uk

[1] Wolfson School of Mechanical, Electrical and Manufacturing Engineering, Loughborough University, Loughborough, Leicestershire LE11 3TU, UK

[2] NSIRC, TWI Ltd, Granta Park, Great Abington, Cambridge CB21 6AL, UK

[3] LAS section, TWI, Granta Park, Cambridge CB21 6AL, UK

PVC	Polyvinyl chloride
PVDC	Polyvinylidene chloride
PVDF	Polyvinyldene fluoride
UF	Ureaformaldehyde
UV	Ultraviolet

1 Introduction

Surface texturing is a surface-modification technique used to improve the performance of materials for various applications. It involves creating textures with fine features on the surface of a material with the aim to impact surface functionalities. Depending on the texturing technique employed, different texture types and sizes can be produced. The influence of texture patterns on surface functionalities may be expressed as a function of feature geometry and/or surface chemistry. In polymers, the process of formation or breakage of bonds in addition to surface roughness, surface energy, and capillarity may result in the surface being either more hydrophobic or hydrophilic. Also, feature geometry influences the adhesive properties of a surface by either reducing or increasing the contact angle (CA) between a liquid droplet and the material surface. This is not in isolation to the increased specific surface-area contributions of micro- and nanostructures [1]. The tribological performance of surfaces is also enhanced by surface roughness created during surface texturing. Surfaces may also be textured for aesthetic purposes. The process of texturing mostly involves material removal by micro-milling or ablation. Whatever the approach employed, precision is the key.

There are a few works summarizing laser surface texturing (LST) of polymers in recent years [2–5]. In this review, an overview of micro-texturing techniques is provided, highlighting their drawbacks, and discussing the ways to eliminate these shortcomings through an in-depth analysis of LST. As this study is focused on polymeric materials, an overview of relevant polymer properties affected by laser irradiation is presented in Sect. 2, while Sect. 3 discusses the ablation mechanism and the influence of the incubation effect on the ablation threshold. This section also describes in detail the principle of each LST technique along with their capabilities and potentials. A critical comparison is done to provide more information on the efficiency of each technique for industrial applications. In Sect. 3.7, the effect of laser parameters on ablation rate and surface features is discussed in depth together with their influence on polymer properties and performance. Finally, based on this review, the authors present the challenges and give suggestions for future work. The last section summarizes the review and its findings.

Over the years, different texturing techniques were explored. Among these techniques are electrochemical machining, micro-milling, ion-beam etching, hot embossing, lithography, mechanical texturing, and LST. A combination of grafting and texturing to improve the wettability and tribological properties of polymer brushes [6] was explored with the aim of prolonging their life. Results of the process showed that the micro-textures protected the brushes from wear and increased their tribological performance, hence extending their service life. Unlike most techniques, which involve material removal, hot embossing is basically the stamping of a pattern on a softened polymer surface [7]. This technique is ideal for mass production because it is fast and relatively low-cost. However, hot embossing involves several temperature and pressure regimes, making the process cumbersome. Electrochemical machining is an easier technique to manage. It is mostly applied to conductive materials as the material removal process is through anodic dissolution [8]. However, a modified version of this process known as 'electrochemical-electrodischarge machining' can be applied to polymers. In this process, polymer surface ablates by temperature increase and heat release that accompanies electrical discharges [9]. LST, on the other hand, is a one-step non-contact process. So far, in comparison to other surface-modification techniques, LST offers more advantages. These advantages include optimal material utilization, reduced processing costs, minimal heat-affected zone, and high product quality. While the capabilities of LST are known, its potential is still being explored. It is true that the process of photolithography is effective in creating precise incisions on a substrate using a single-laser beam. However, this processing method requires a completely flat substrate surface and an environment that is free of contaminants [8]. Unlike photolithography, focused ion beam milling is a mask-less process that uses ion particles. The challenge of this technique is due to the scattering of resulting particles. This 'scattering effect' leads to unwanted particle deposition on the treated surface thereby causing property modification. However, more ion beam irradiation is required to remove the deposited particles [10]. In contrast to ion beam machining, electrochemical-electrodeposition machining produces surfaces with high surface integrity. The downside of this method is the thermal nature of the process which induces cracks and alters the mechanical properties of the polymer. Hot embossing is another good replication technique for producing micro-components on a large scale based on time and cost. However, the major drawback of this process is in the demoulding stage. In this final stage, the replicated structure may get damaged as a result of the applied force during the separation of the mould and the substrate [7]. Most shortcomings of these surface processing techniques are absent in the LST. As mentioned earlier, the advantages of LST outweighs those of the other processes, thereby making it a preferred alternative for polymer surface texturing. Schematics of these texturing processes are presented in Fig. 1.

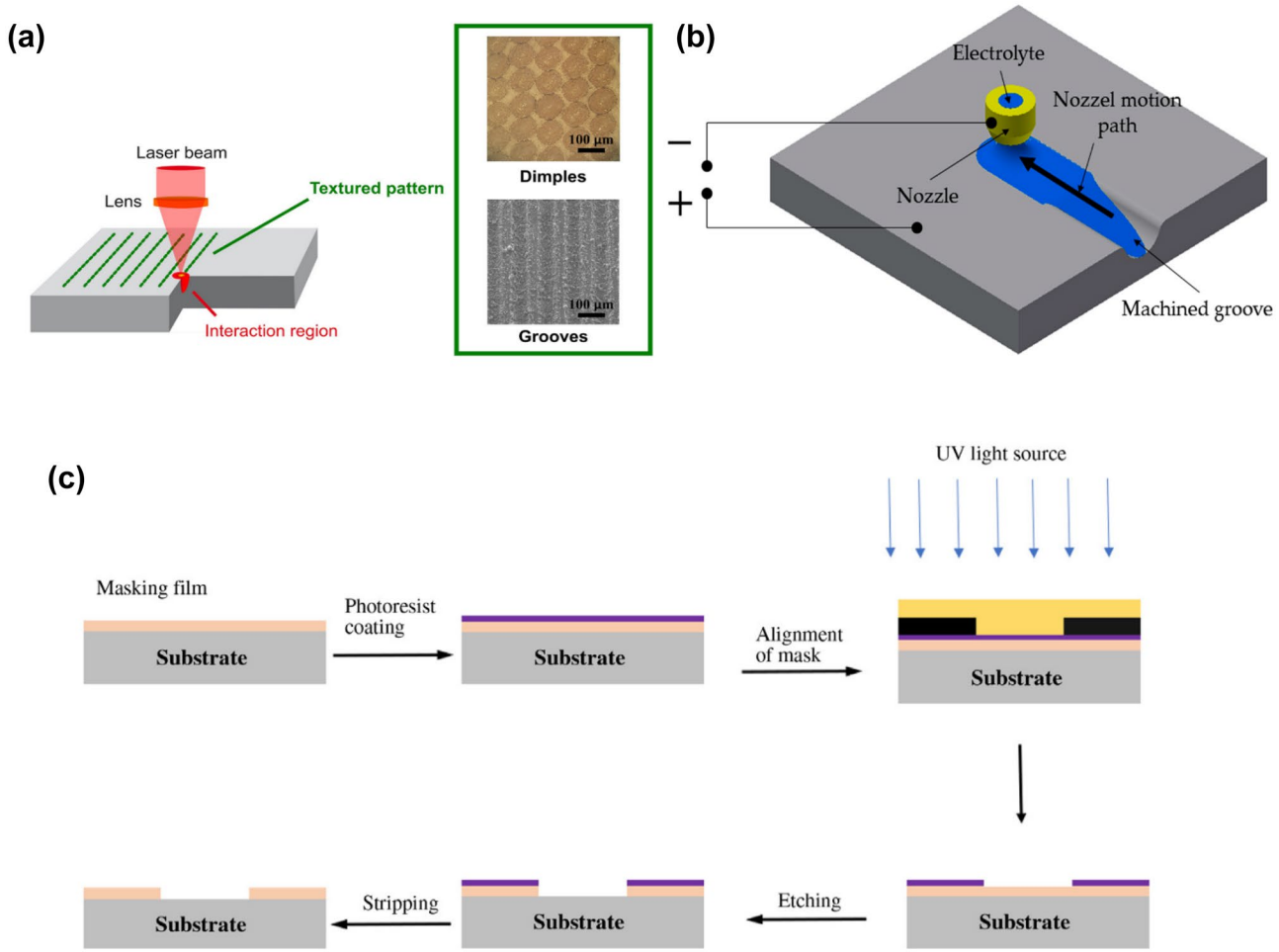

Fig. 1 Schematics of some polymer micro-texturing processes. **(a)** Laser-beam micromachining/laser writing [2]. **(b)** Electrochemical machining [11]. **(c)** Photolithography [12]. **(d)** Ion beam etching/milling (1) milling; (2) deposition; (3) implantation; and (4) imaging [13]. **(e)** Hot embossing [14]

This section has looked at other surface texturing methods applied to polymers with the aim of improving surface functions. The method involved in these processes has been given but kept brief as the paper focuses on micro-texturing methods using lasers. The drawback of these non-laser processes was discussed briefly, while the capabilities of LST were highlighted. Since the materials of interest are polymers, the next section looks at their properties that are affected by laser, how they are affected, and the implication of these effects. Properties such as optical and mechanical ones are seen to be the most affected by laser irradiation. The behaviour of polymers under applied stress is analysed alongside the optical behaviour of laser-irradiated polymers

2 Polymer properties influenced by laser irradiation

Polymers used in engineering applications are mostly synthetic with either linear, branched, or cross-linked structures (Fig. 2). The forces of attraction between polymer chains determine polymer properties [15]. Laser interactions with polymers alter specific properties as a result of chain scissions and cross-linking. Cross-linking enhances the physical and light-transmission properties of polymers but reduces their crystallinity. Generally, the response of polymers to laser is influenced by the nature of the polymer and parameters of the laser beam. Although the primary outcome of light absorption is free electrons or phonons and not heat, the long interaction time associated with long laser pulses produces heat from the collision of these free electrons. Heat energy transfer through the polymer matrix from absorption and collision of photons leads to rapid temperature rise within the bulk. Depending on the amount of energy input, thermal degradation may occur. Using different investigation techniques, changes in the optical or physical properties of polymers indicate whether cross-linking or degradation dominated during laser irradiation. Reports showed, for instance, that the refractive index of a nuclear track detector comprising polyallyl diglycol carbonate is dose-dependent [16]. Just

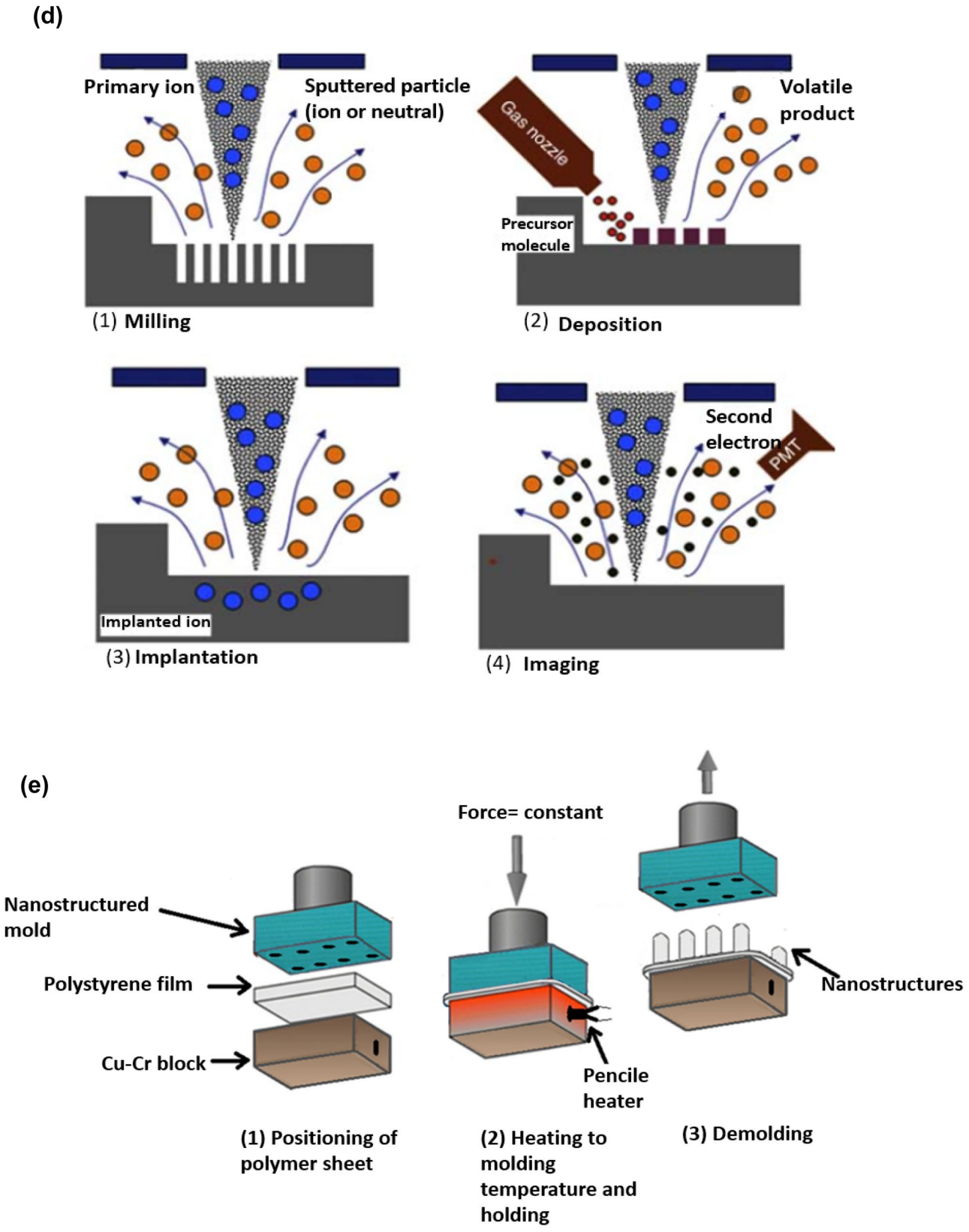

Fig. 1 (continued)

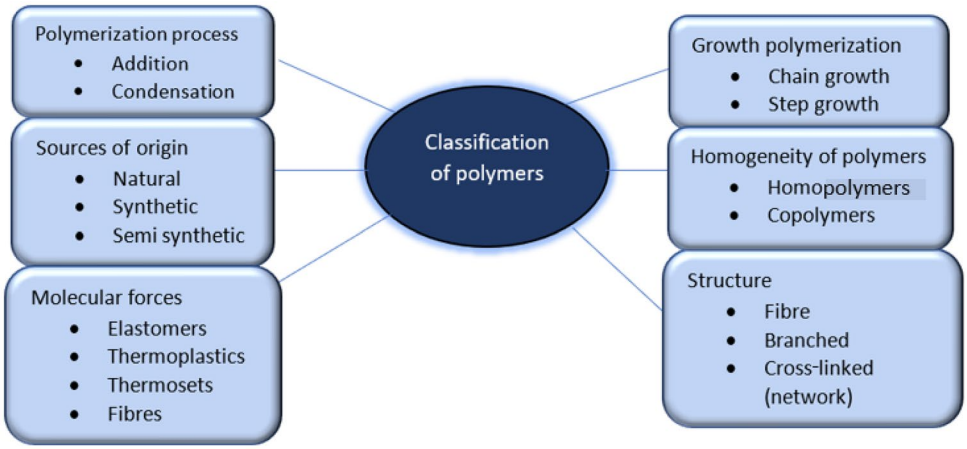

Fig. 2 Polymer classification (adopted from [18])

like other optical properties, the refractive index depends on several factors such as wavelength, temperature, and optical frequency. Since the visible spectral region lies within the region of strong absorbance, the refractive index increases at shorter wavelengths [17].

Mechanical properties of polymers are also influenced by laser. Naturally, attraction forces between atoms and nearby molecules along with the movement of molecule segments greatly affect the mechanical properties of polymers [15, 16, 18]. Intermolecular forces depend on the nature of polymer atoms and can be altered by irradiation-induced cross-linking or bond scission. The behaviour of polymers under applied stress varies depending on the polymer type and the extent of laser-induced changes. The most popular method of investigating mechanical properties is by performing stress–strain analysis. The stress–strain behaviour of polymers is sensitive to parameters such as molecular weight. The molecular weight of a polymer provides some knowledge on the polymer's origin and method of polymerization. A direct relationship exists between the molecular weight of a polymer and its tensile strength because an increase in the former enhances the latter up to a point of saturation. At a lower molecular weight, polymer chains are held loosely by weak van der Waals forces of attraction, causing the chains to move effortlessly at some levels of crystallinity [18]. On the other hand, large chains in polymers with high molecular weight are entangled, providing the polymer with strength. Laser-induced degradation can be used as a rapid method of studying the aging or radiation stability in polymers [16]. In untreated polymers, the deformation curve (Fig. 3, curve C) shows that elastomers demonstrate total elasticity or rubber-like elasticity with large recoverable strain at low applied stress levels. Under higher stress levels, some polymers deform elastically (Fig. 3, curve B) until a certain point, when they start to undergo plastic deformation. Highly plastic materials exhibit necking for an extended period after the yield point is reached. On the other hand, brittle polymers do not show significant strain levels at increased stresses (Fig. 3, curve A), and a further increase in stress then causes their abrupt failure. The stress–strain behaviours described in Fig. 3 may be enhanced or marred by laser irradiation.

Reports showed a relationship between ablation and glass transition temperature (T_g). In the ultraviolent laser irradiation of polymethylmethacrylate (PMMA) film, PMMA undergoes expansion with increasing fluence above 0.4 J/cm^2 [19]. The temperature recorded at this fluence level was about the same as its glass transition temperature (105 °C). Since PMMA is amorphous, it is brittle, rigid, and hard. Upon heating an amorphous polymer, molecular chains twist around each other, making the polymer soft and flexible; this takes place at T_g. During glass transition in semi-crystalline polymers such as polyethylene terephthalate (PET) and polytetrafluoroethylene (PTFE), only the amorphous regions undergo the transition, while the crystalline regions are unaffected (Table 1) [12].

The properties of polymers affected by laser irradiation were discussed briefly in this section. The mechanism, by which these changes occur, was analysed alongside its implication on optical and mechanical properties. Since laser irradiation affects the physical properties of polymers, a table with physical properties of common biomedical and industrial polymers is included. The next section is focused on laser texturing techniques starting with a detailed explanation of ablation mechanism in polymers. An in-depth discussion of the direct laser writing (DLW) and direct laser interference patterning (DLIP) methods is provided to highlight their capabilities and potential.

3 Laser surface texturing techniques

3.1 Laser-induced ablation of polymers

Laser ablation is the process of surface modification by material removal. Ablation occurs when the target material

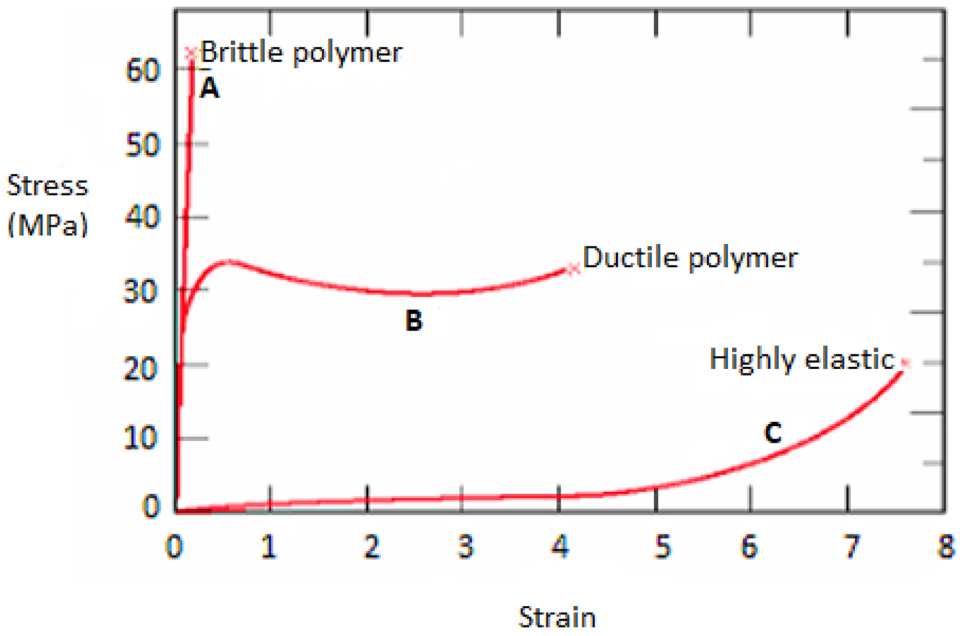

Fig. 3 Polymer behaviours under applied stress. Polymers can display brittle behaviour **(A)**, plasticity **(B)**, or high elasticity **(C)** [18]

absorbs energy from laser irradiation such that the energy of its atoms or ions becomes higher than their binding energy, resulting in phase transformation. Laser pulse duration and intensity together with material physical properties determine a material's response to laser irradiation, resulting in different regimes and mechanisms governing the material removal process [26, 27]. For ablation to occur, an energy threshold needs to be exceeded. In laser ablation, fluence (J/cm^2) is the energy of a laser pulse incident on an area of a material surface and can be calculated [28].

$$F_i = \frac{4P_m}{\pi d_i^2 f}, \qquad i = 1, 2..5 \tag{1}$$

where P_m is the average laser power (W), d_i is the radial position on beam spot diameter (cm) at varying positions (i) from 1 to 5, and f is the frequency (KHz). Fluence can also be estimated as the maximum value in the middle of the laser path. Given that the peak intensity (I_{max}) of a Gaussian beam is

$$I_{max} = \frac{2P}{\pi {w_0}^2} \quad , \tag{2}$$

Table 1 Physical properties of polymers influenced by laser irradiation during LST [20–25]

Polymer	Glass-transition temp, T_g (°C)	Melting point (°C)	Ultimate tensile strength (MPa)	Yield tensile strength (MPa)	Thermal conductivity (W/m K)	Specific heat capacity (J/g °C)
PTFE	−97	330	33.6	11.6	0.27	1.4
PP (isostatic)	+100	160	13.8–460	12–43	0.11–0.44	1.92
PS	90−95	240	44.9	43.9	0.14	2.1
PMMA (atactic)	+105	270	75.0	75.4	0.2085	1.46
Nylon 6,6	+57	250	73.1	45–63.6	0.26	2.2
LDPE	−20	110	11	10.8	0.3	2.2
HDPE	−90	120–140	30.5–35	26–33	0.48	1.9
PP (atactic)	−18	160	36.8	30.7	0.11	2.0
PC	+150	288–316	64	62	0.2	1.2
PE	+69	260	51.8		0.05	1.87
PVC	+87	100–260	1.38	55	0.190	0.84–1.17
PSU	+190	332–371	72	74.9	0.22	1.2
PEEK	+140	+340	110	98.8	0.25	2
PVDF	−37.6	160	42.8	44–48	0.19	1.5

maximum fluence will be.

$$F_{max} = \frac{2\sqrt{2}}{\pi w_0} \times \frac{P}{v} \tag{3}$$

where P is the laser power, v is the scan speed, and w_0 is the beam radius at the focal plane [29]. This implies that the beam radius/waist is given as 2 w_0.

The magnitude of fluence necessary for ablation to happen is influenced by the material's absorption mechanism, the presence of defects, the surface morphology, the microstructure, and laser parameters such as wavelength and pulse duration [30]. A proper model for material ablation must take into account the volume of material that absorbs energy, the thermal energy loss by the material, and the required amount of energy for phase transformation to occur [31].

The mechanism of ablation depends greatly on the absorption of energy from a focused laser beam by the topmost layer of a material or a substrate. Polymers absorb the laser energy in a non-linear manner compared to metals. Ablation includes both vaporization and melt ejection from the focal area [32]. If the energy of an incident laser beam is less than the ionization potential of the polymer-bound valence electrons, vaporization will not occur. However, impurities or inclusions that are present in all materials serve as sources of free electrons, which are inherently absent in polymers. These impurities or inclusions are usually fewer in number than the valence electrons and are not tightly held like the bound valence electrons. When the free electrons get hit by energetic photons in the laser beam (e.g., ultraviolet lasers), they absorb energy by collision in a process known as *inverse bremsstrahlung* leading to the breaking of chemical bonds [27]. This photon-electron excitation produces heat when long laser pulses are used. This energy absorption agrees with the Beer-Lambert law, which states that the quantity of energy absorbed depends on laser light intensity and the thickness of the material [4].

Photoionization is the first step in a laser-induced material breakdown (Fig. 4). During photoionization, valence electrons absorb enough energy from incident laser photons to move to the conduction band. In this band, free electrons are generated by multiphoton ionization or by impact ionization. At increased kinetic energies, subsequent collisions of energized free electrons result in the emission of secondary electrons through inverse bremsstrahlung absorption. This leads to an avalanche growth in the number of free electrons and, finally, material removal through melting or vaporization as in the case of infrared (IR) radiation [34, 35]. In contrast to IR radiation, ultraviolet (UV) radiation is capable of ionizing and decomposing polymers with minimal melting, making such radiation a preferred option in LST [35, 36].

The ablation process can be photochemical, photothermal, or both, depending on parameters of the laser technique and material properties such as reflectivity, pulse duration, absorption coefficient, and wavelength [37]. In the photothermal process, the energy from laser pulses increases the surface temperature of the material, leading to melting and vaporization. Photothermal processes induce surface modifications such as roughness in polymers. However, in the photochemical process, there is a direct breakage of molecules by highly energized photons incident on a material surface, hence inducing chemical modifications. This is mostly achieved using lasers with wavelengths within the ultraviolet region of the light spectrum. The combination of both photothermal and photochemical processes modifies the roughness and chemistry of surfaces simultaneously [2].

3.2 Ablation threshold

An ablation threshold is useful in evaluating the success of a material removal process. As fluence is the total laser energy over an irradiated area, the ablation threshold is the maximum energy that a material can withstand without ionization

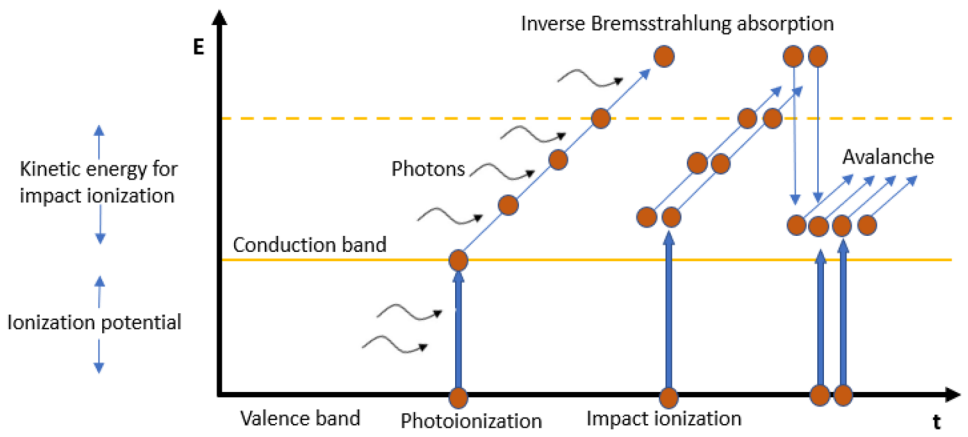

Fig. 4 Schematics of photoionization, inverse bremsstrahlung, and impact ionization during laser-induced breakdown process [33]

[31]. A low ablation threshold implies that a small amount of energy is required to produce noticeable changes on an irradiated material surface. Hence, the ablation threshold is the fluence value, above which ablation occurs. Generally, the threshold fluence for inorganic insulators and organic materials (polymers) is between 0.5 and 2.0 J/cm^2 and 0.1 to 1 J/cm^2, respectively [30]. Fluence measurements in pulsed laser ablation are computed for individual pulses rather than the fluence over the total time as is the case of continuous waves. This is because the ablation threshold reduces as the number of repetitive laser pulses increases due to the incubation effect (i.e., shielding of subsequent pulses by initial incident pulses). This implies that laser fluence below the threshold value has the capability to modify a material surface. Hence, a study of the extent to which the incubation effect influences ablation process is essential. A relationship between the single pulse $F_{th}(1)$ and the multi-pulse $F_{th}(N)$ ablation thresholds is given by [30]

$$F_{th}(N) = F_{th}(1)N^{\xi-1} \quad , \tag{4}$$

where F_{th} is the ablation threshold, and ξ denotes the degree of incubation and can be obtained from the gradient of the graph of log $[N\,F_{th}(N)]$ and logN. It is important to note that in the case of absence of the incubation effect, $\xi = 1$ [30]. A material softens at ξ values between 0 and 1 [38] and hardens at values greater than 1. Theoretically, the ablation threshold tends to zero with an infinite number of pulses as can be seen from Eq. (4); this means that as the number of pulses increases, this equation becomes less applicable.

In the previous studies, the most widely studied polymeric substrates were polymethylmethacrylate (PMMA), polyethylene (PE), polycarbonate (PC), polyfluoroethylene, and polyimide (PI) [39]. The contribution of the incubation effect to ablation was observed in the femtosecond-laser treatment of some polymers. The findings revealed the transition in the absorption mechanism of the transparent polymers [31]. Multiphoton absorption took place during single-pulse ablation. When multiple pulses were irradiated, the absorption mechanism became linear. In polymer substrates with high fluence thresholds, a considerable amount of energy is transferred to the material, resulting in heating, boiling, vaporization, and pore formation (Fig. 5a) while a small portion of the laser energy goes above the region for material ionization. On the other hand, a greater portion of the pulse energy is permitted above the ionization/material removal barrier eliminating the boiling phase as observed in Fig. 5b. The porosity created on PE after laser surface treatment can be attributed to rapid cooling of the super-heated melt after intense boiling.

In the micromachining of polymer substrates using femtosecond lasers, a comparison of the behaviour of urethane-based amorphous co-polymers to similar homopolymers was conducted [39]. Scanning electron microscopy (SEM) images revealed the presence of pores in the microstructure produced by ablation using a 275 nm wavelength femtosecond laser beam. Unlike the homogenous surface structure achieved with a 550 nm laser beam, a diverse range of surface morphologies caused by re-solidification of the melt was observed when the copolymer was irradiated with a 275 nm femtosecond laser beam. The experimental results revealed an increase in the ionization threshold fluence with increasing wavelength regardless of the number of pulses. The description of a similar relationship led to the observation that the homopolymers absorbed laser energy better when irradiated with 275 nm than with 800 nm laser beams, leading to a reduced ionization threshold fluence [31].

Different microstructures obtained with laser irradiation at 800 nm (Fig. 6) and the resulting colour alterations were recorded at different fluences. At fluences below $F_o = 1.3$ J/cm^2, ablation did not occur; rather, porous structures were formed in all the polymeric samples with an obvious loss in transparency observed only in polytetrafluoroethylene, PC, and polylactic acid (PLA) below the ablation threshold. A gradual darkening was revealed until PC turned black. Upon increasing the fluence, PLA,

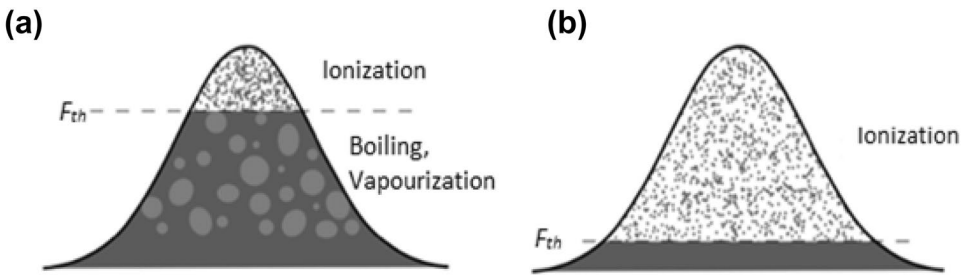

Fig. 5 Influence of fluence threshold on temperature of re-solidifying melt. Polymer substrates with high fluence thresholds **(a)** undergo isovolumetric material heating, boiling, and vaporization resulting in pore formation. **(b)** Materials with low fluence thresholds undergo ionization and material removal [31, 39]

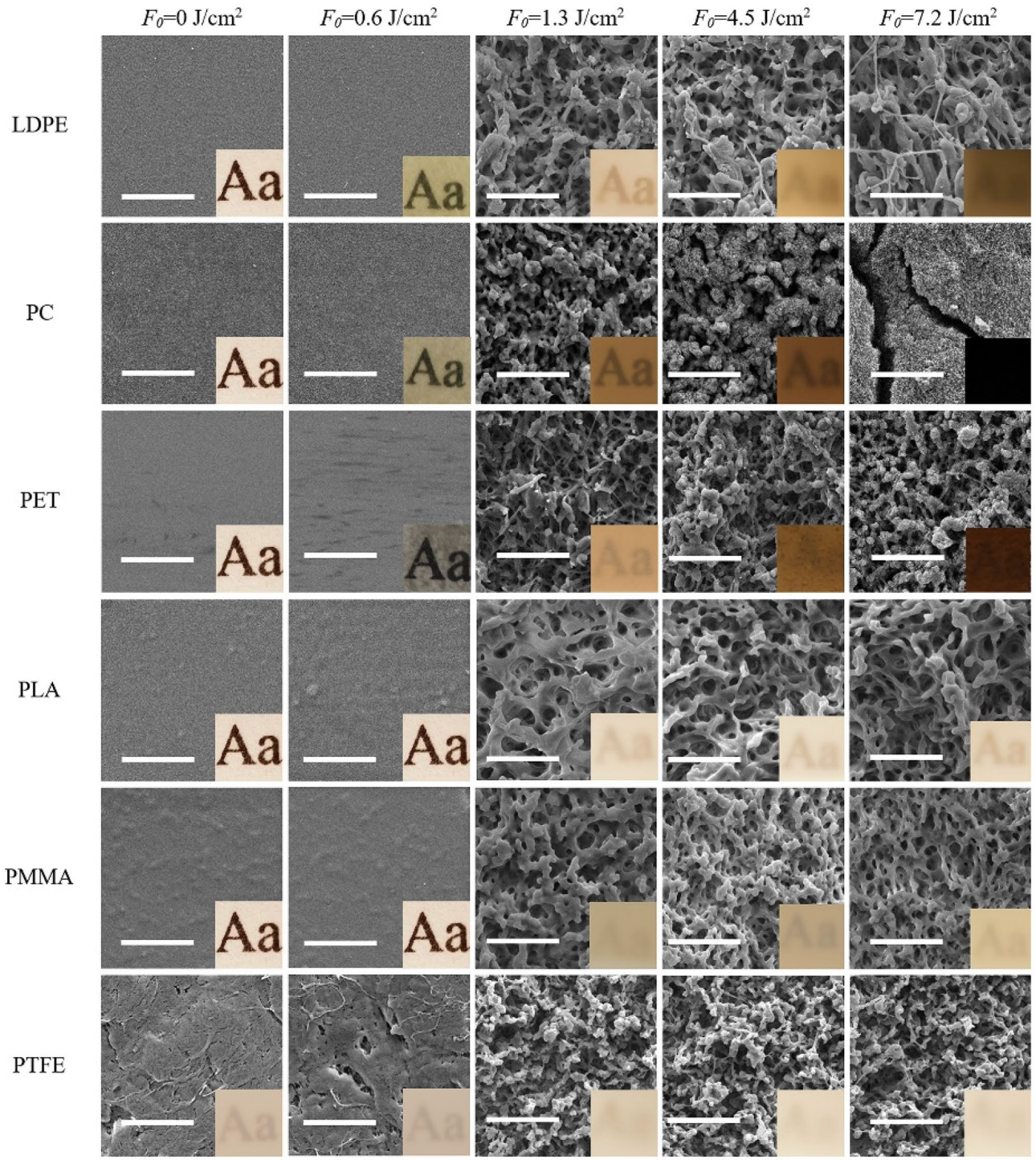

Fig. 6 SEM images of microstructures produced with wavelength of 800 nm on different polymers at various fluences [31]. A 3 mm×3 mm photograph insert of the sample on a white paper with letter imprints indicates the variation in transparency [31]

polytetrafluoroethylene (PTFE) and PMMA did not exhibit any structure or colour change [31].

Unlike the case of the 800 nm wavelength (Fig. 6), the formation of microstructures at lower fluence (Fig. 7) implies a reduction in threshold fluence, when a wavelength of 275nm was used. Formation of particle clusters was clearly observed on PC, while PTFE sustained a similar structure and colour at both wavelengths. Polyethylene terephthalate (PET) remained transparent at all fluences, with small melt lumps on the surface, which turned

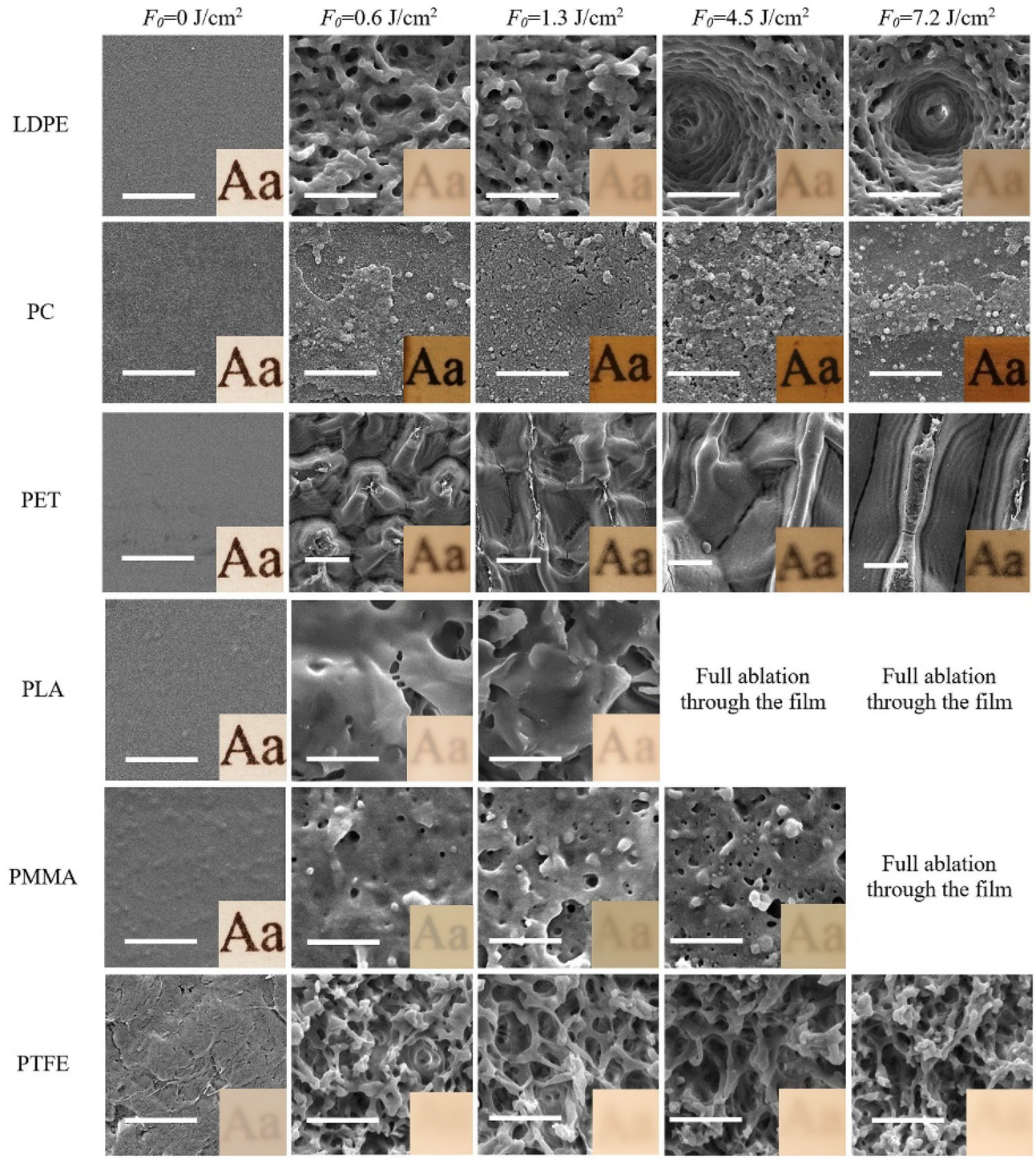

Fig. 7 SEM micrographs of laser-induced microstructures at 275 nm wavelength for various fluences. A 3 mm × 3 mm photograph insert of the sample on a white paper with letter imprints indicates the variation in transparency [31]

into grooves at increased fluence. Full ablation (perforation) through the film was observed in PLA and PMMA at fluence levels above 3.3 J/cm^2 and 5.8 J/cm^2, respectively. This simply means that the high fluence values used was high enough to induce ablation through the relatively smaller thickness of the PLA (75 µm) and PMMA (50 µm) films used for the experiments. A visible melt layer with a small amount of porosity was observed in all materials. However, in low-density polyethylene (LDPE), circular-shaped craters with increased porosity were formed in

different sections of the surface at $F_o \geq 4.5$ J/cm^2 [31]. The authors concluded based on visual inspection that the optical properties of LDPE, PC, PET, PLA, PMMA, and PTFE were altered by the laser machining process. In this study, it was observed that an increase in wavelength from 275 to 800 nm at 55 pulses per spot led to an increase in the fluence threshold in all the polymer substrates. Since almost all the investigated polymer materials were transparent and so had large bandgaps, the ablation behaviour can be said to have occurred by multiphoton absorption.

Irrespective of the fluence, the absorption coefficient of every material is unique at different wavelengths. The literature shows that most polymers have better absorption at UV wavelengths. This explains why all the polymers in this study displayed either a porous structure or a visible melt layer at 275 nm for all fluence values when compared to the 800 nm wavelength. A graphical comparison of fluence thresholds of all the polymers at two studied wavelengths is shown in Fig. 8. PTFE and LDPE demonstrated the highest threshold fluence and maintained a porous structure at the 275 nm wavelength. The third highest fluence threshold at this wavelength was PMMA, which displayed a lower level of porosity, while PLA, PET, and PC revealed considerably lower threshold values at 275 nm. Therefore, it is safe to associate the formation of laser-induced porous structures in polymers with the ablation threshold fluence at the operating number of pulses per spot. The surface structure observed in the different polymers at the 800-nm wavelength was not very dissimilar. These structures which looked like clusters of resolidified melts might be due to localized boiling, which is typical with high-threshold fluence. High-threshold fluence of materials usually amounts to a small amount of the laser energy above the required threshold for ionization and material removal [39].

Porosity detected on the sidewalls and the bottom of the ultrashort laser-ablated PMMA surface structures are a result of trapped bubbles, which occurred during re-solidification of the melt layer [40]. This interpretation is in agreement with the numerical simulations carried out for PMMA by [41]. Hence, the reliance of threshold fluence on the operating conditions is elucidated supposing that the formation mechanism of the laser-induced microstructures observed in Fig. 7 is similar to descriptions in other research works [40, 41]. Similar to this research [31], the dependency of the ablation threshold on a number of pulses incident on one spot for PC and PMMA substrates [40] was demonstrated. The variation in laser fluence from $0.5 - 2.5$ J/cm^2 was attributed to the incubation effect. Laser ablation was carried out on these two polymers (PMMA and PC) using a Ti: sapphire laser system with a pulse duration of 150 fs, at 800-nm wavelength, pulse energy of about 750 µJ, and repetition rate of 2 Hz (Figs. 9 and 10).

There was no noticeable material removal or redeposition of molten material around the circumference of the laser spot after the first pulse (Figs. 9a and 10a); instead, material swelling was observed in the beam's spot area. This was due to polymer fractionation, CO–O bond breakage (usually supported by XPS data), and CO_2 vapour evolution that escapes in a localised surge. As the number of pulses increased, vapour pressure built up enhancing the process

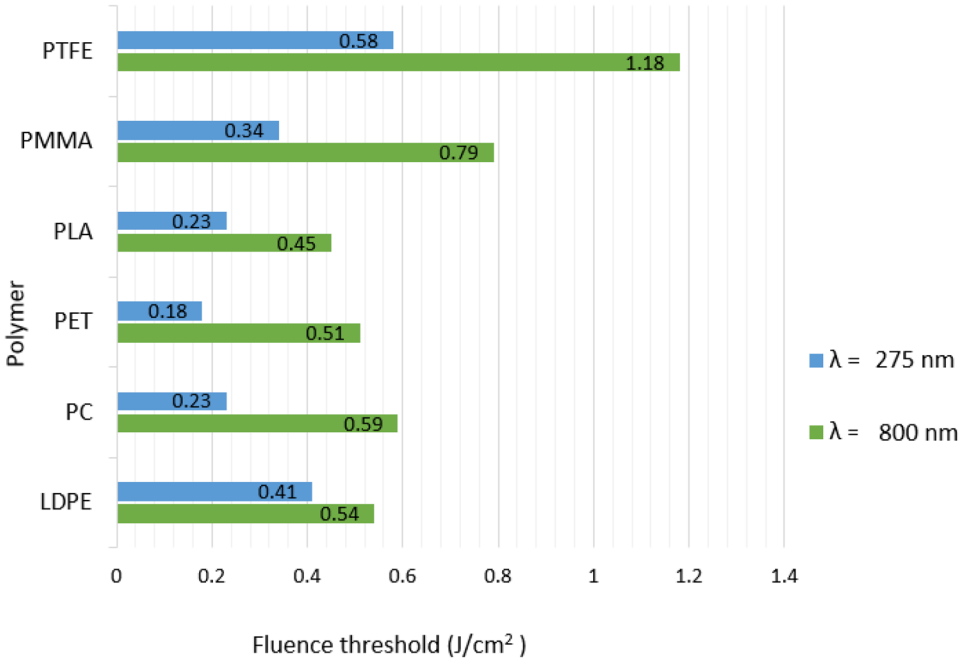

Fig. 8 Comparison of threshold fluence after irradiation of 55 pulses per spot at $\lambda = 275$ nm and $\lambda = 800$ nm (adapted from [31])

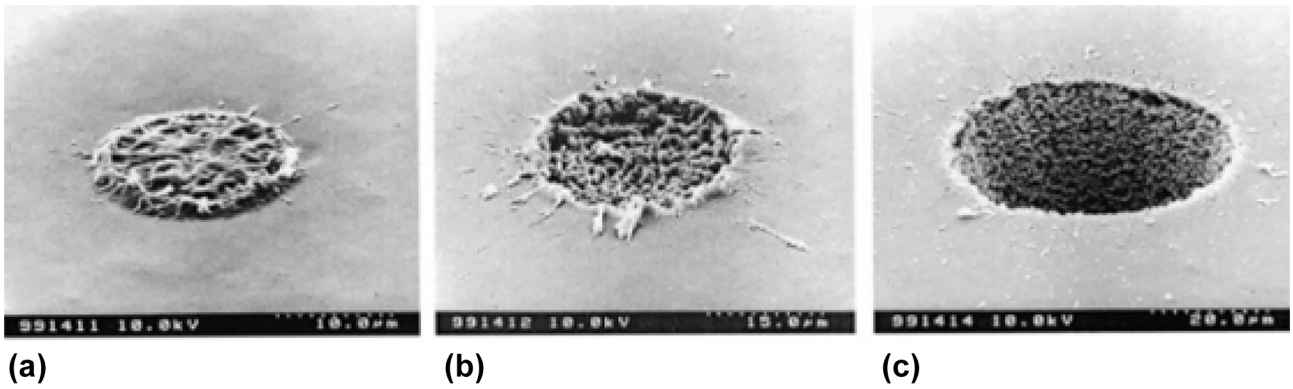

Fig. 9 SEM micrographs of PMMA surfaces after laser irradiation (pulse duration 150 fs, wavelength 800 nm, threshold fluence 3.0 J/cm^2) for different number of pulses: **(a)** 1; **(b)** 5; and **(c)** 100 [42]

to a point where material ejection from the surface of the substrate became possible (Figs. 9c and 10c).

3.3 LST by direct writing

For several last decades, scientific interest in mimicking complex structural orientations observed on naturally occurring surfaces was on the rise. The research community did considerable work in this area, but the morphological complexity of the features posed a challenge in trying to successfully fabricate a replica of naturally occurring textures on engineering materials. Several approaches were adopted among which ultrafast laser direct writing is the most common [3]. Laser direct writing, commonly referred to as direct laser writing (DLW), is a flexible, high-precision contactless processing technique that uses focused laser beams to write complex structures efficiently over large surface areas of materials. It involves moving a focused laser beam across a material surface in a line-wise manner at a precise speed and number of pulses per spot [43]. DLW is defined as a 3D photolithography technique, which creates very tiny features by the solidification of a photoresist at the focal point of a laser beam [44]. However, there seems to be slight differences in the definition of DLW by different authors. The first approach in DLW [3] involves inducing hierarchical micro- and nano-surface structures using an ambiance of a reactive etching gas, mostly sulphur hexafluoride, SF_6. Although this approach was adopted and [45] found to be successful in improving water repellence on a black silicon surface, the technique is limited by the size of produced features. This limitation can be resolved by another laser texturing technique known as the direct laser interference patterning (DLIP), where multiple features can be created within a single spot. The second approach involves an initial creation of an ablation pattern using a laser beam and then applying different laser parameters to decorate the unaltered areas with laser-induced surface structures [46, 47]. This approach is similar to laser-beam micromachining, with microfeatures fabricated on material surface by utilizing laser beam properties to achieve control and avoid any damage to surface integrity of the target material [30]. The final approach is a time-consuming spot-by-spot

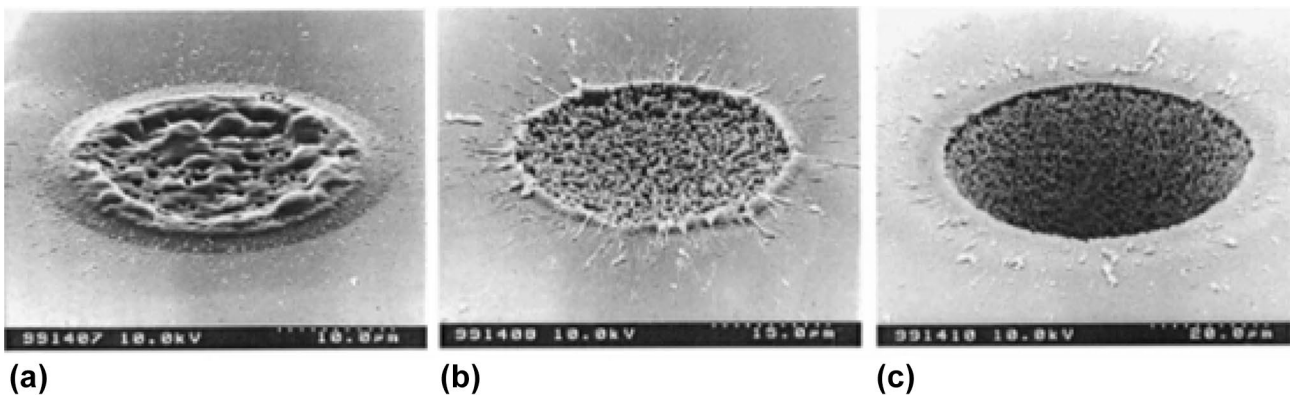

Fig. 10 SEM micrographs of PC surfaces after laser irradiation (pulse duration 150 fs, wavelength 800 nm, threshold fluence 3.0 J/cm^2) for different number of pulses: **(a)** 1; **(b)** 5; and **(c)** 100 [42]

cylindrical-vector-beam irradiation to produce controlled and precise surface structures with multiscale spatial frequency [43, 48]. In this approach, cylindrical vector beams are used to fabricate primary microstructures, which are then decorated with secondary submicron undulations. The height of micro-cones produced and the distance between the features can be altered by varying the incident angle and the pulse overlap. Multi-scale frequency structured surfaces exhibit remarkable wetting characteristics, exploited for a wide range of applications [48].

3.4 Optical setup

In an ultrashort pulsed DLW setup (Fig. 11), an ultra-short, pulsed fibre laser and 2D scanner are connected to a computer that controls the operations. In this arrangement, the polymer substrate is stationary as the beam movement is controlled by the scanner. In other setups, a two-axis moveable stage, a beam expander, or a mask may be incorporated. The laser head delivers the collimated laser beam to the writing head, where the movement of the mirror(s) is manipulated. In setups with a beam expander, it is positioned at the beam discharge point of the laser head and the entry point of the scanner. The beam expander is mostly used to vary the focus spot size of a focusing lens to maintain the beam collimation in systems with long beam paths. Texture parameters such as scan path, hatch type, hatch distance, and hatch arrangement are controlled with the scanner software, while the sample is placed on a stationary stage. However, in setups with a sample on a moveable stage, the beam is kept stationary.

Ultrashort laser pulses are used in laser micro-machining applications because they offer high energy intensity and, thus, precise laser-induced breakdown threshold at reduced fluence. Other advantages of ultrashort laser pulses include reduced adverse thermal effects and damage, high spatial resolution, and improved quality of ablated features. Ultrashort laser processing of transparent materials by strong-field ionization is obtainable thanks to the high peak intensity of ultra-short pulses. Strong field ionization is the first step in multiphoton ionization, which is mostly associated with high-intensity optical laser fields of short duration [50]. The major shortcoming of DLW is the difficulty to fabricate a tiny surface features at high processing speed, as creating small structures involves sequential writing with a very close laser focus or a small spot size [3]. Millions of convex microlens arrays on PMMA were manufactured with a femtosecond DLW (FDLW) method [51]. The fabrication process was based on a single femtosecond pulse in-situ modification without incorporating masks or duplicated templates. The authors achieved their aim in developing an efficient approach for generating convex microlens arrays on a large surface area of the PMMA sheet. Results of their experiments showed that in 1 h, millions of lens units could be fabricated on PMMA effortlessly. At a pulse energy less than a damage threshold, the absorption mechanism was mostly due to multiphoton and avalanche ionization. Further exposure of the polymer to laser irradiation resulted in the breakup of polymer chains. In line with [52], the regions of PMMA surface under direct laser exposure were observed to undergo localized swelling. In addition, a uniform surface finish of several stable microlens was maintained until ablation began to occur as pulse energy increased to a threshold value. Pores were formed at the top of the dome-shaped micro-lens, which grew in size with increase in ablation. Craters were formed from material expulsion due to plasma production [51]. Obviously, pulse-energy alterations influence the extent or type of surface modification that may be achieved on a polymer surface. An elongation pattern of

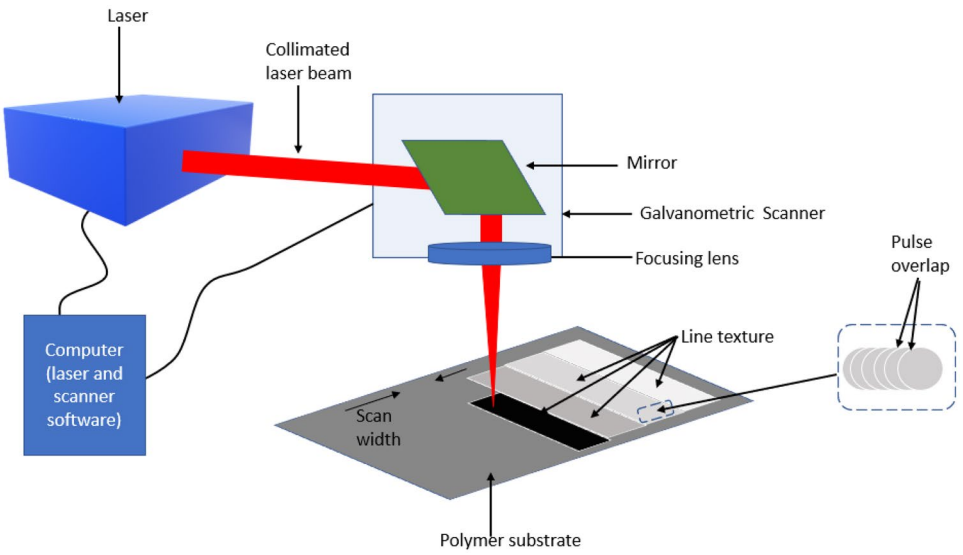

Fig. 11 Schematic of a simple DLW setup using laser pulses to depict 'writing' of line features on polymer surface. Adopted from [49]

the ablation craters was observed at increasing pulse energies [41]. Research findings indicate that ablation craters formed at higher pulse energies propagated in the direction of laser-beam polarization. Asymmetric ablation craters are produced at linear and elliptical beam polarizations at twice the threshold fluence, while circular polarization gives rise to symmetric craters.

As stated above, the fabrication of micrometre and submicrometre surface structures can be done by different technologies. The major challenge is not only to fabricate these structures but to produce them at low cost and high throughput. Just like most laser surfacing techniques with their unique drawbacks, the DLW approach is a relatively slow process because of the need to draw each feature sequentially [3]. The processing speed of photolithography and DLW is in the range between 0.01 and 200 cm^2/min [53]. In addition to the challenge associated with processing speed, the resolution of the features that can be produced with the DLW technique is limited (down to 10–20 µm). Resolution control is influenced primarily by the laser spot size which depends on the beam diameter, wavelength, focal length, and numerical aperture of the focusing lens [54]. Precision micro-machining of periodic structures by interference field of laser beams is a much faster alternative route for producing features with resolution below 10 µm [53, 54]. The major difference between DLW and DLIP is that the latter permits parallel surface processing by the interference of two or more coherent laser beams [3].

3.5 LST by DLIP

DLIP is an efficient LST approach that employs the interference of coherent laser beams on a material surface to create a periodic pattern of structures with high resolution [55]. This technology is effective for fast patterning of large surface areas with features down to nanometre-scale [55, 56]. The DLIP process provides better flexibility in the choice of target material and texture geometry. Intricate patterns of dots and lines can be produced with the DLIP method since the shape and spatial periods of the features are determined by the number of laser beams used, the intensity or polarization, and alterations in the interference angle of the incident beams [57]. The DLIP method was shown to be effective in treating different materials and in creating advanced structures for a large variety of applications such as in optoelectronics, manufacturing of micro lenses, improvement in the growth of nanorods, and tissue engineering for sensing humidity and producing scaffolds [56, 58–60]. Processing speeds of 0.36 m^2/min and 0.9 m^2/min can be achieved on metals and polymers, respectively [53, 55].

3.6 Interference principle and optical setup

In the DLIP process, a single beam is split into two or more beams that are made to overlap on the surface of a target material to produce an interference pattern. As a result, the optical set for DLIP is different from that for DLW. In the latter, the output laser beam from the laser head is focused directly to a suitably small spot on the surface of the substrate using a mirror or an objective lens at normal or angled incidence. The working distance and the minimum achievable spot size on a substrate are dictated by the numerical aperture, or F number, of the lens (a ratio of a focal length of lens to input laser-beam diameter at lens) [61]. Using mirrors, the laser beam is directed to the DLIP optical head. The main element of the DLIP system is a diffractive optical element (DOE), which splits the collimated laser irradiation into different beams (referred to as *sub-beams*) at an angle. The split sub-beams pass through a wave plate (full, half, or quarter) for further beam polarization and are then parallelized by a prism. The parallel sub-beams are made to overlap using a converging lens at a known focal length to create an interference in the focal region, where the sample/substrate is placed. In some cases, filters or beam expanders are incorporated in the DLIP setup to reduce (or increase) the beam intensity either to minimize material damage or to obtain the adequate energy for texturing to take place. The distance between the DOE and the prism can be varied to alter the intensity profile at interference [62–64]. To set the accurate working distance between the laser head and the substrate, the sample is usually placed on a movable stage (x, y, and z directions).

In a basic optical setup of a DLIP system (Fig. 12a) and the interference fringe pattern (Fig. 12c), produced at the sample surface, the actual surface texturing takes place in the interference volume (Fig. 12b). Selective ablation occurs at the maxima positions of the intensity distribution produced when the adequate energy is applied. If the DLIP setup is configured for two sub-beams, periodical line-like structures are formed on the substrate surface [54]. The distance between these periodic line-type features is known as *spatial period* Λ and can be calculated using the following equation [54]:

$$\Lambda = \frac{\lambda}{2sin(\theta/2)} \quad , \tag{5}$$

where λ is the wavelength of the laser beam and θ is the angle between the interfering sub-beams.

Depending of the number of interfering sub-beams, a variety of feature shapes can be produced. This was demonstrated in several works using six and four sub-beams [65, 66] to fabricate cross-like holes, elliptical holes, and circular holes on different materials. Three symmetrically

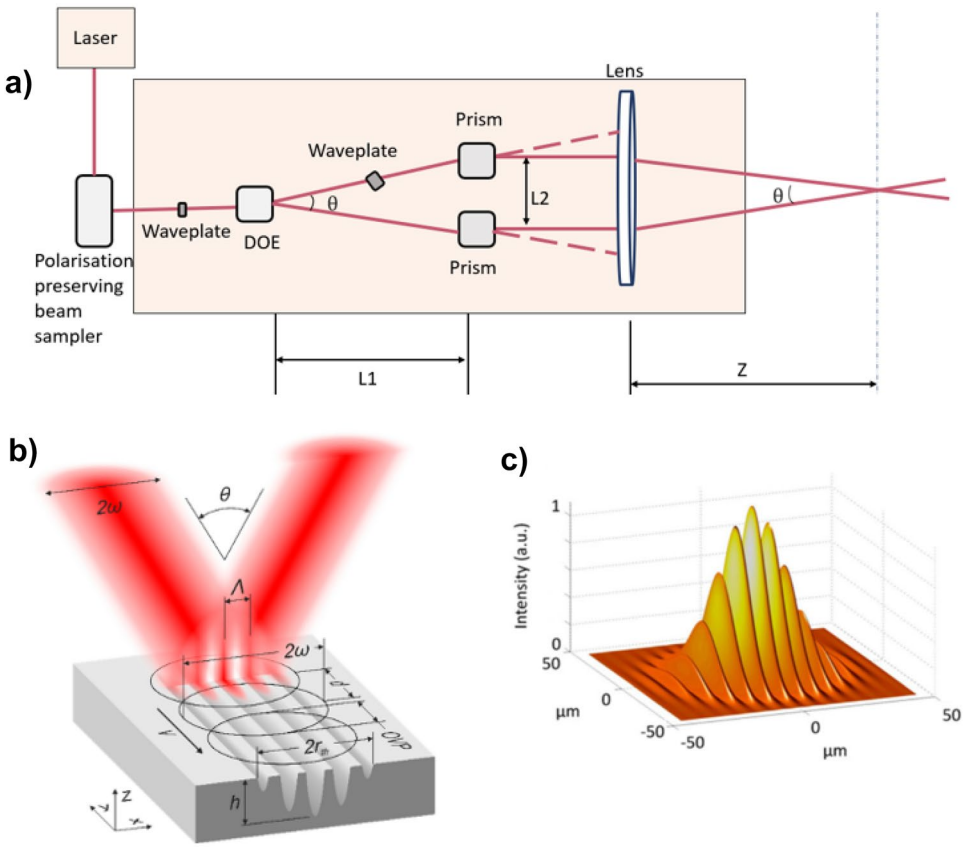

Fig. 12 **(a)** DLIP experimental setup showing optical elements for the two-beam interference pattern. **(b)** Two-beam direct laser interference patterning process. (Λ—laser intensity profile/ablated structure period; ω—laser beam radius; θ—beam intersection angle/incident angle; d—distance between the laser spots; rth—radius of ablated area; OVP—spot overlap; v—translational speed of samples; h—depth of ablated structure) [64]. **(c)** Calculated beam-intensity distribution obtained from overlap of two Gaussian (TEM_{00}) [56]

arranged sub-beams were employed in [67] for the production of a dot-shaped interference pattern with a hexagonal intensity distribution. From Eq. (5), it is clear that the minimum achievable pitch for $\theta = 180\ ^\circ$ and $\lambda = 1064$ nm is 532 nm. Larger surface areas can be textured by moving laser spots in the y-direction (Fig. 12b). Laser pulses released at a specific repetition rate f are displaced at a distance d which can be calculated as [55]

$$d = \frac{\nu}{f} \quad , \tag{6}$$

The spots overlap (OVP) can be calculated as a function of the distance between laser pulses d and the beam radius ω as [55]

$$OVP = 1 - \frac{d}{2\omega} \quad . \tag{7}$$

This implies that the displacement distance d of laser spots can be expressed as a function of (OVP) as follows [55]:

$$\mathrm{d} = 2\omega(1 - \mathrm{OVP}) \quad . \tag{8}$$

It is important to note that the laser-beam radius is equivalent to the radius of the spot created on the substrate's plane. In theory, the shape of the spot on the substrate surface is elliptical rather than circular when the interference angle θ is large. Therefore, at small θ values, the ellipticity of the spot can be overlooked [55].

Investigations of the mechanism of DLIP involved in structuring pigmented and transparent PC substrates using UV and IR laser radiations [56] demonstrated the occurrence of two ablation mechanisms in the transparent PC. This transparent PC selectively ablated at maxima positions (areas of maximum interference) at low laser fluence when the spatial periods, corresponding to the distance between features, were large. The resulting surface comprised well-defined patterns when the adequate laser energy was utilized. On the other hand, at high fluences and short spatial periods, a structure geometry merging a periodic distribution and a Gaussian-like swelling was produced due to the erasing of the upper part of the periodic modulation. The second mechanism that was observed by the authors was swelling, unique to the black-doped PC with IR wavelength, resulted from the detachment of the polymer dopant, forming pores (Fig. 13d).

A better understanding was obtained from the analysis of the absorption spectra of the textured materials in the region between UV to near-IR. Unlike the transparent PC,

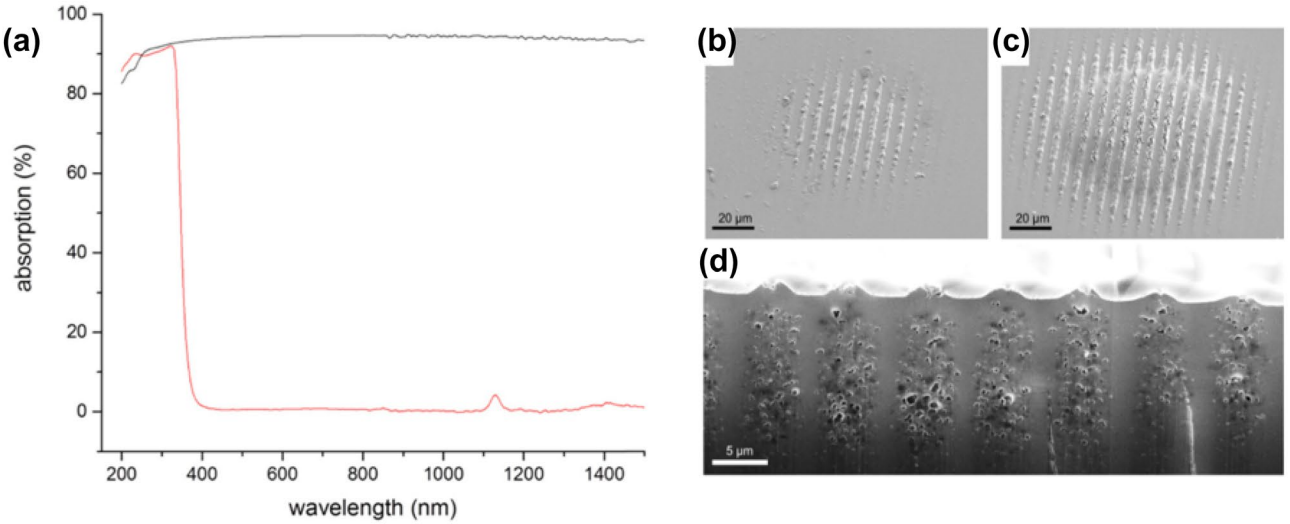

Fig. 13 **(a)** Absorption spectra of transparent polycarbonate (red line) and black-doped PC (black line) for wavelength range between 200 and 1500 nm. SEM images of DLIP-treated black-doped PC using a wavelength of 1053 nm and fixed spatial period of 7.13 µm. **(b)** Single-scale line-like ridges at fluence of 0.86 J/cm^2. **(c)** Swelled double-scale structure at fluence of 1.3 J/cm^2. **(d)** Focused-ion-beam cross section of swelled double-scale pixel at laser fluence of 1.3 J/cm^2 (reprinted with permission from [56])

which exhibited insignificant absorption at wavelengths longer than 400 nm, the pigmented PC displayed an almost uniform absorption between 200 and 1400 nm spectral range as shown in Fig. 13a. Therefore, the swelling process can be linked to the absorption of IR photons by the black dye, which then formed gaseous by-products, creating pores, and, finally, resulting in a localized volume increase. Lastly, the authors developed a model for predicting the contribution of different structuring mechanisms (ablation and swelling) in the direct laser interference structuring of any polymer substrate [56].

In a similar work [53], topographical analysis of fabricated micro- and sub-micrometre features on PC with DLIP were carried out using SEM and confocal microscopy. To gain a better understanding of the mechanism with which the structures were created, a focused ion beam was employed to produce cross-sections of the treated surface (Fig. 14).

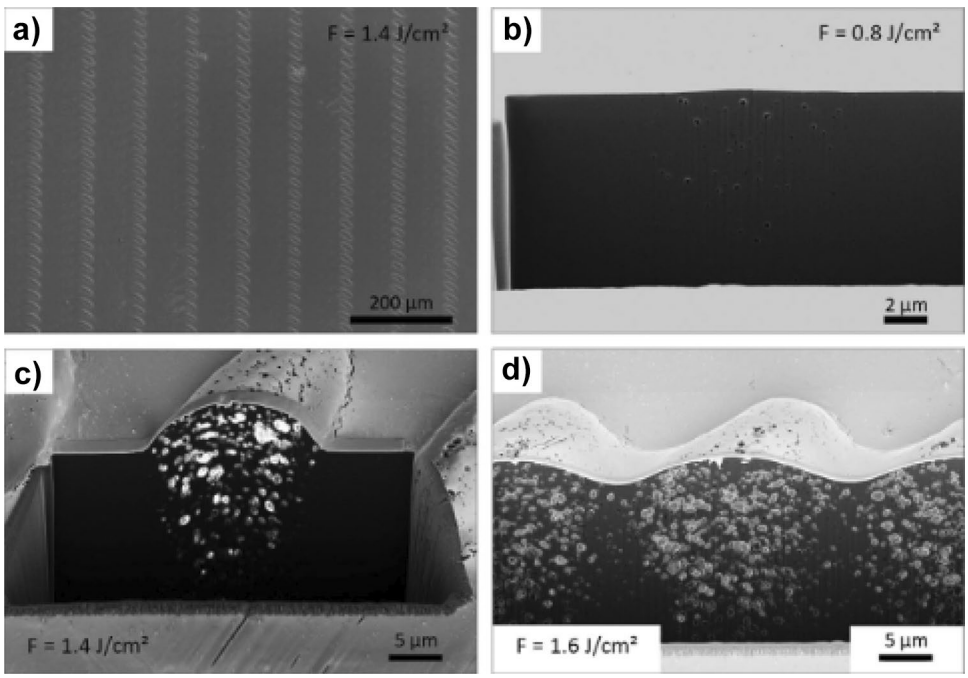

Fig. 14 SEM images of DLIP of carbon-doped PC. **(a)** Top view of pattern. **(b–d)** Cross-sectional view of patterns obtained with focused ion beam [53]

The homogenous topography of the elliptical pattern contour at a fluence of 1.4 J/cm^2 (Fig. 14) is an indication that focus diameter was greater than the DLIP pitch. Cross-sectional views at a tilt angle of 36 ° in Fig. 14 reveal the production of pores and induced swelling in the carbon-doped PC substrate. The assumption is that there was an interaction between the dopant and the laser. Thermal decomposition then took place as the absorbed heat energy was transferred to the PC matrix.

3.7 Comparison of fabrication speed for DLW and DLIP

A comparison of fabrication speeds offered by DLIP and DLW provides an insight into the potentials of DLIP and DLW, where cost is a critical factor. The time to create features on a surface using DLIP is considerably shorter than that for the DLW process. Consider a square area of size S on a material surface to be textured with features having a period P, the time t_{DLW} required for the fabrication of these structures with DLW can be expressed as [66]:

$$t_{DLW} = \frac{S^2}{vf} = \frac{S^2}{P^2 f} \quad , \tag{9}$$

where v and f are the fabrication speed and the laser repetition rate, respectively. This implies that it will take over 17 h to texture a surface area of 25×25 cm^2 with a feature period of 1 µm and a repetition rate of 1 MHz. From Eq. (9), the time required to structure an area in DLW can be decreased by increasing the pulse repetition rate and the scanning speed using fast beam positioning systems such as polygon scanners. However, the challenge with high repetition-rate lasers is that they often possess smaller pulse energies which are inadequate for direct material ablation to take place. Also, the laser beam focus with polygon scanners is mostly to large spot sizes within the range of tens of µm which determines the smallest achievable feature size and period [66].

Since DLIP offers the possibility of structuring large areas using only a single high-energy laser pulse, the time needed for the fabrication of the same area 25×25 cm^2 with a 1 µm structure period and a repetition rate of 1 kHz using a single laser spot (1 mm) can be computed as [66]

$$t_{DLIP} = \frac{S^2}{vW} = \frac{S^2}{W^2 f} \quad , \tag{10}$$

where W is the diameter of the single laser spot. From, the time to accomplish this fabrication is 63 s. While the processing time of both DLIP and DLW depends on the pulse repetition rate, it is evident from Eqs. (9) and (10) that the DLIP fabrication time depends on the laser spot size while that of DLW depends on the feature period. A direct comparison to determine which process is more efficient based on the structure period can be obtained using the following equation [66]:

$$P_0 = \frac{v_{DLIP}}{v_{DLW}} W = \sqrt{\frac{f_{DLIP}}{f_{DLW}}} W \quad . \tag{11}$$

Hence, for the features with periods smaller than P_0, the DLIP method is more suitable while for bigger structure periods, DLW technique is more efficient.

The graphical comparison of fabrication time against structure period for DLW and DLIP techniques at different repetition rates (Fig. 15) [66] indicates that with the DLW process, an increase in the laser repetition rate from 1 to 100 MHz reduces the time required to fabricate features of a particular period on a 25×25 cm^2 surface area. On the other hand, since the DLIP fabrication time is independent of structure period, the fabrication time is constant at varying structure period.

In this section, the mechanism of ablation was discussed. The concept of incubation was introduced here along with its influence on the ablation threshold and the overall LST process. Maximum energy input required for ablation to occur was presented. The absorption coefficient and optical behaviour of different polymers varies at different wavelengths. The direct writing and direct interference patterning methods of laser surface texturing were also discussed in depth. An explanation of both techniques, their optical setup, and some patterns obtained on polymers were presented as well. The method, which allows manipulation of the spatial period for features produced with the DLIP technique, was presented along with the relevant equations for LST with DLIP. A comparison of the processing speed and times was made for both techniques to serve as a guide. The next section looks at the influence of laser parameters on the LST process. Parameters such as wavelength, pulse duration, ionization energy, number of pulses, absorption, and fluence are discussed in terms of ablation rate and type of surface features produced.

4 Effects of laser parameters on the surface texturing process

Laser parameters and material properties play an essential role in the ablation of organic materials with short pulses. These parameters include, but are not limited to, material type, reflectance, absorption coefficient, thermal conductivity, laser-pulse duration, wavelength, and laser-pulse energy [67].

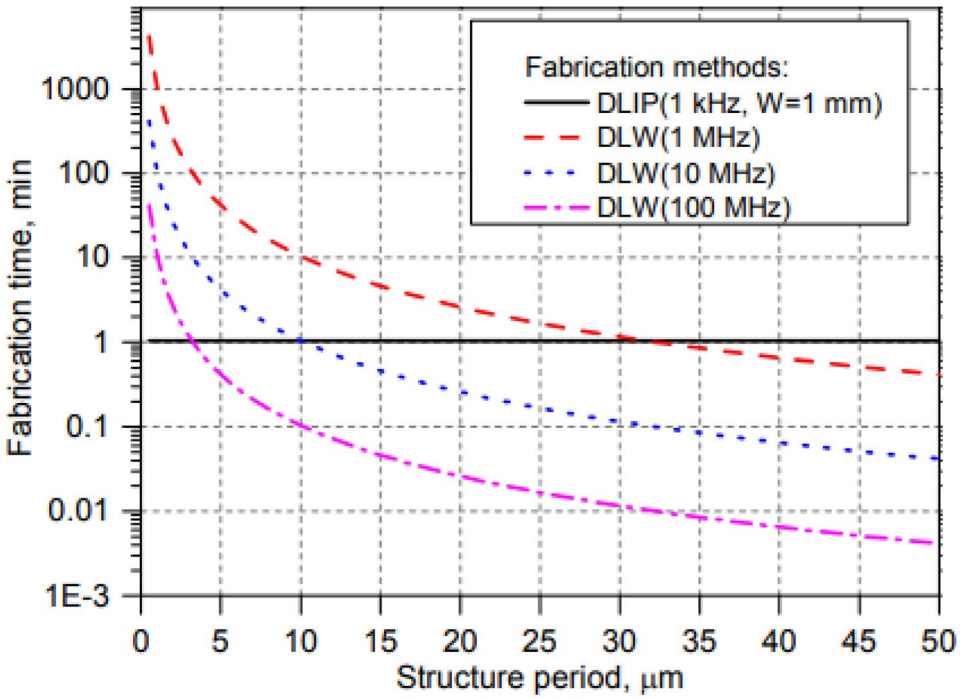

Fig. 15 Effect of fabrication time on structure period for area of 25 × 25 cm^2 using DLIP (repetition rate 1 kHz; spot size 1 mm) and DLW (repetition rate 1 MHz and 100 MHz) [53]

4.1 Influence on ablation rate

In polymers, the most important factor that determines the feasibility of creating periodic patterns with DLIP is the ability of the polymer to absorb the laser energy (absorption coefficient) at a given laser wavelength [35]. Polymers generally exhibit very good photon absorption in the UV spectra range. Surface texturing of polymers using UV radiation leads to ionization and disintegration of polymeric materials without significant melting. The use of far-UV radiation creates well-defined pits on the surface of polymer substrates in a process known as *ablative photodecomposition* [35]. This is not the case for the wavelength into the visible or infrared region, where the material is damaged as a result of distortion, melting, and charring [36]. The absorption of laser energy by Teflon in the IR spectra is reported to be weak. Teflon shows an increasing ablation coefficient with a decrease in the wavelength when measured using photothermal beam deflection at various wavelengths. The photothermal deflection technique is a useful method to obtain the ablation threshold for different materials by measuring the deflection of a probe beam resulting from the refractive index slope of a target surface generated by a modulated beam [68]. For absorption of laser energy, an understanding of the effect of heat transfer by thermal conductivity in the material becomes critical. The time scale associated with short pulses minimizes the energy loss by heat diffusion helping to reduce cracking and presence of a recast melt layer, and produces features with high aspect ratios. The previous research proved that during the ablation of high-molecular-weight polymers, a molten material with high viscosity is produced, which results in the reduced of ablation rate [69]. Investigations on the ablation of PTFE with 248 nm laser pulses produced from an excimer laser [70] revealed the chemical degradation at a fluence of 2 J/cm^2 after 50 pulses for a pulse duration of 16 ns. In another experiment with shorter pulses of higher intensities (300 fs, 1 J/cm^2), the material removal process in PTFE did not result in any thermal damage. Unlike PTFE, other polymers like PMMA display changes in optical properties—from transparent to strongly absorbing of 248 nm wavelength—due to chemical modifications from the incubation effect that takes place within the first few laser pulses. The authors reported the threshold fluence of PTFE to be roughly 0.5 J/cm^2 for a pulse duration of 300 fs.

Several researchers investigated the influence of wavelength on ablation rate for polymers. In the work by [71], the rate of ablation of sintered PTFE was observed to increase initially, followed by a decrease as the wavelength was increased. The relationship between the ablation rate and the wavelength is independent of the laser fluence. Measurements of the ablation threshold of PTFE (Teflon) at different wavelengths were recorded [68] with a further attempt to predict the absorption coefficient at individual wavelengths. Reports showed a decrease in the wavelength, which led to an increase in the absorption coefficient of PTFE. Due to the very low absorption coefficient of PMMA, structuring the polymer at high laser intensities using wavelengths such as 266 nm and 355 nm and single pulses becomes difficult [67]. However, in strongly absorbing polymers such as

polystyrene, the rate of ablation depends on pulse duration and laser fluence. The dependence of ablation threshold on laser wavelength in PI was investigated [72] in processing with an excimer laser. These investigations demonstrated that in the etching of PI, the presence of oxygen did not alter the etching/ablation rate but oxidized the ablated features. For the same polymer, a photoacoustic spectrometer was used to evaluate the influence of pulse duration on the ablation rate [73]. At a pulse duration between 7 and 300 ns for a XeCl laser, the ablation depth was measured from 0.1 to 1 μm for each laser pulse. However, the dependence of the ablation threshold on pulse duration was observed to be weak. The ablation rate of PI showed a very rapid rise above threshold fluence of 0.1 J/cm^2 to an 80% saturation point at 0.5 J/cm^2 for a 355-nm wavelength (Nd: YAG laser) and 30-ps pulse duration [74]. The reflectivity (fluence-dependent), the photoacoustic signal and the intensity of emission were recorded to provide an insight into the saturation mechanism. The term *saturation* used here is as in the incubation effect, where the plume (ablated species) created by the leading edge of a pulse prevents the trailing end of the pulse from reaching the substrate through absorption. Further radiation absorption by the plume results in excitation and release of more photons. If the plume completely blocks the rest of the photons from getting to the substrate surface, an increase in photoacoustic signals was still below the saturation fluence. Although there are arguments on the possibility of radiations with intensities below the ablation threshold leaking through the plume to cause an increase in photoacoustic signals, this is not applicable because the signal levels identified below the ablation threshold are too low to explain the rise above the saturation point. Another argument is that fragments produced from subsequent absorption by the plume may collide with the substrate and create acoustic signals. However, the possibility of this occurrence is very low, since the plume's upstream density should be extremely high so that only the fragments nearest to the substrate can collide with it [74]. In addition to saturation of the ablation rate, the authors also observed that the debris formed from the ablation process had an influence on the morphology of the ablated polymers.

4.2 Effect on surface features

The study on laser processing of Teflon in ambient air using Ti: sapphire femtosecond laser with 780-nm wavelength [75] revealed that, at high fluences, the ionization effect by air decreased the efficiency of the ablation process and reduced the quality of the ablated features. The ablation depth was observed to increase with an increase in the number of pulses. In a similar experiment [76], the ablation threshold of PET for 50 mm Ti: sapphire laser with two different pulse durations—200 ps and 80 fs—was examined. The authors reported that with former duration and at a fluence threshold of 8 J/cm^2, cracks developed on the surface, alongside non-uniform holes formed from ablation. On the other hand, 80-fs laser produced clean holes and uniform cuts at a fluence threshold about five-folds less than that necessary for ablation with 200-ps laser pulses. Research on femtosecond DLW on PMMA in [51] demonstrated the effect of laser-pulse energy on the shape and size of the fabricated convex microlens arrays. The authors reported an initial increase in the height and diameter of the convex microstructures as the laser power increased from 1 mW (at laser fluence and laser intensity of 39 mJ/cm^2 and 0.78 TW/cm^2, respectively) to 2 mW (with corresponding laser fluence of 79 mJ/cm^2 and laser intensity of 1.58 TW/cm^2. Afterward, the height decreased with increasing laser power to 5mW (with equivalent laser fluence of 198 mJ/cm^2 and laser intensity of 3.96 TW/cm^2). Generally, the morphology and geometry of laser-induced surface features vary with laser power. Morphological changes occur due to the temperature distribution and transport of species in the substrate [77].

As mentioned above, the interference of two or more coherent beams in DLIP on a material surface produces periodic patterns with controlled pitch and geometry. In the same DLIP process, the shape of the features is defined by the number of laser beams and the intensity or polarisation of the laser beams used, while a manipulation of the angle between the incident beams controls the spatial period of the produced features [56, 57]. This is the reason for creation of more complex periodic structures using the DLIP process as opposed to the DLW or single-beam laser machining. The depth of fabricated features determines the processing speed to a large extent since more laser pulses per spot are required to create deeper structures. Therefore, to fabricate features with increased depth, a higher amount of laser energy is required, resulting in reduced throughput [63, 64, 78–80]. Laser fluence—in addition to the distance between pulses—also affects the structure depth and the quality of features. Investigations on the homogeneity of features produced with the DLIP process were carried out in [63], and the importance of process optimization to achieve uniformly distributed features over a patterned area was demonstrated. DLIP has been used to create diffraction gratings on transparent PET substrate for the use in packaging and consumer goods [80]. Experimental results [63, 80] reveal that an increase in the number of pulses and the pulse energy led to an increase in the structure depth caused by a comparable increase in the ablated material. This agrees with other works. However, an inverse proportion was noticed with a further increase in the number of pulses and the pulse energy, resulting in a decrease in the structure depth. The reason for this change can be attributed to the molten material moving into the valleys of the pattern. By optimizing the process parameters through design of the experiment approach, the authors

concluded that diffraction efficiency of treated PET was strongly dependent on the height of the fabricated surface structures. Other works showed that a pulse-to-pulse overlap had a strong effect on structure depth. Generally, high pulse overlaps can produce deeper features if the applied energy density is adequate. The temperature gradient also plays a role in determining texture homogeneity and can be controlled by pulse overlaps. Melting or ablation caused by irradiation of a polymer surface with an interference pattern depends on the pulse duration, which, in turn, influences the energy flow from positions of interference maxima to those of minima or the cooler regions and bulk [79]. Also, heating in minima positions may occur when interference patterns with short spatial periods are used. This reduces the thermal gradient and the flow of the molten material, thereby giving rise to structures with reduced height [81]. In addition to this, [82, 83] reported that material vaporization, supported by recoil pressure, reduced the quality of microstructure by the turbulent flow of the molten material.

In summary, different process parameters influence the laser texturing process as well as the features produced on polymer surface. Since the features formed are linked to the process parameters, the resulting surface functionalities are dependent not only on surface morphology and feature geometry but also on these parameters. In the literature, the exact feature morphology or geometry produced with LST of polymers (that impact specific surface functionalities) remains unclear. Another factor that influences LST is environmental conditions. Oxidizing or neutral atmospheres play a role in determining the outcome of texturing processes, but the previous works are scarcely investigated and/or reported. Figure 16 highlights some features commonly obtained in most laser-textured polymers. Due to the absorption mechanism and polymer's response to laser irradiation, discrete spots, grooves, conical features, or hierarchical structures may be produced in polymers. It is misleading to assume that the application of the same process parameters used on metal substrates would yield similar results in polymers. While distinct features with similar parameters may be obtained on different metals, polymers would behave differently. In some cases, a laser-irradiated polymer with only slight surface modifications (such as surface melting, solidification, and redeposition as in Fig. 16g, h) may offer the same functionality as a metal with clear grooves, laser-induced periodic surface structures (LIPSS), or dimples. This is mostly observed for high-peak power lasers, where the energy is absorbed by the material without exceeding the ablation threshold. Research clearly links the impressive functionalities of some laser-modified polymer surfaces to surface chemistry changes, estimated by means of surface free energy calculations and the contributions of the dispersive and polar components to the total surface free energy. Since polymers and polymer composites continue to attract attention of researchers, more work is needed in this area, with a view to

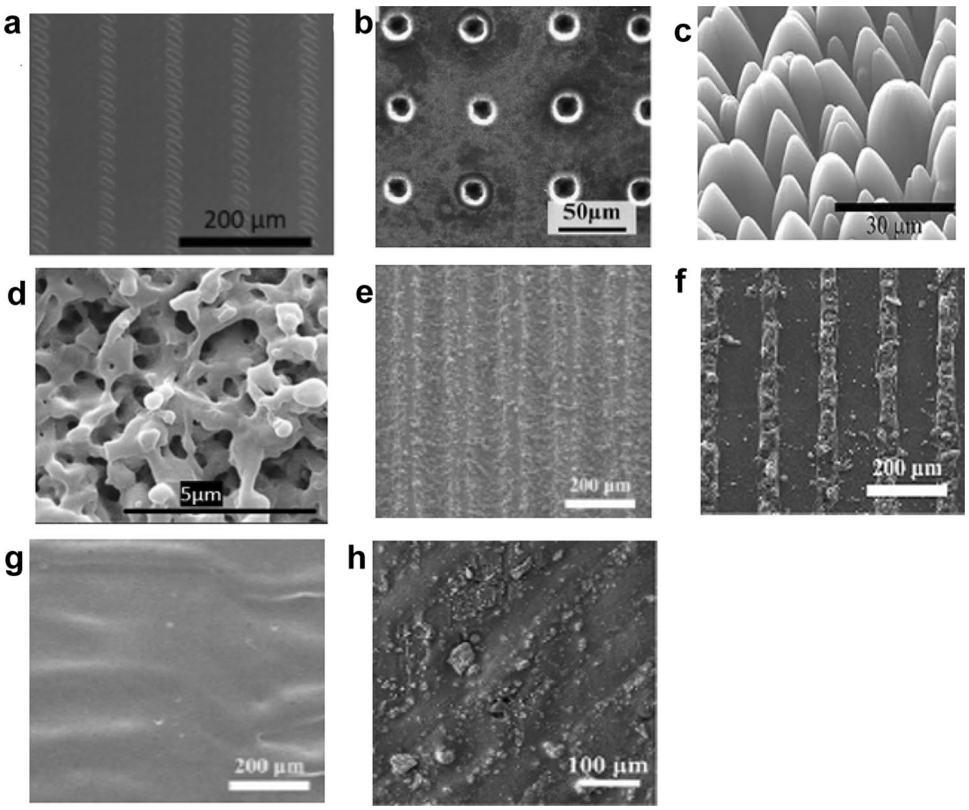

Fig. 16 Scanning electron microscopy images. **(a)** Line-like dots on carbon-doped polycarbonate [53]. **(b)** Discrete spots on polyetheretherketone (PEEK) [84]. **(c)** Conical structures on PI [85]. **(d)** Laser ablated PET [86]. **(e–g)** Grooves, melting with material redeposition and slight surface melting, respectively, on PEEK [87]. **(h)** Laser-modified UHMWPE [88]

optimize the existing texturing techniques and develop more sustainable and robust approaches for texturing of polymers.

5 Influence of textures on polymer-surface properties

Specific surface features induced on polymer surfaces can enhance the performance of that surface. Surface texturing regulates the surface energy and CA, which can result in improved surface hydrophobicity, hydrophilicity, and tribological properties of such polymers [3]. Many plants and animals display unique wetting characteristics thanks to a combination of surface chemistry and structure (or roughness). Animals such as reptiles, birds, and amphibians passively trap water on their body surface. For example, the filefish can swim through oil-spilled waters with oil sliding off its skin from head to tail. The underwater oleophobicity of the filefish is achieved by a combination of anisotropic micro-textures and surface composition. This unique surface property of the file fish can be applied in the design of underwater organic fluid directing and self-coatings for oil pipelines and ship hulls [, 3, 89]. The fibrous structure found on the wings of insects such as dragonfly, mayfly, or a lace wing is responsible for their resistance to wetting. This homogenous surface structure commonly described as an *interconnected netting of ridges* exhibits high CAs of about 150 ° and antimicrobial properties [90]. In 2014, Liang et al. attempted to replicate the fibrous surface structure of insect wings on PTFE using an 800-nm femtosecond laser beam. The resulting structure resembled a forest of entangled fibres, impacting superhydrophilicity of the polymer surface. Further bioadhesion experiments revealed that the 'forest' surface trapped air, thus preventing cell adhesion. Such entangled fibrous surface structures can be employed in biomedical engineering for antiadhesive applications.

5.1 Wetting

A common feature of water-repellent plants is a cuticle, which is composed of a hydrophobic polymeric matrix known as *cutin* covered with waxes. Although the cuticle plays a role in the water-repellent nature of these plants, their unique surface topography also contributes greatly to this effect [3]. The leaf of the lotus plant is a typical example of a super-hydrophobic surface, which also makes it possible for the lotus leaves to remain clean after contamination with dirt. The self-cleaning property of the lotus leaf is primarily achieved by reduced particle adhesion to the leaf surface. The leaf's surface texture is such that there is a limited contact area between the surface and dirt particles or water droplets. This occurs because the droplets are unable to penetrate the nano grooves and rather remain suspended at the tips of the structures. Pockets of air are formed in the space between the water droplet and the leaf surface; thus, a roll-off water droplet picks up any dirt particle as it slides over the leaf surface. This self-cleaning property is popularly referred to as the 'lotus-effect' [3].

A self-cleaning mechanism of the lotus leaf is demonstrated by the roll-off of a liquid droplet on a smooth less hydrophobic surface in Fig. 17. The lotus leaf exhibits particular remarkable wetting attributes derived from very high CAs, usually in excess of 150°, and very small CA hysteresis—usually less than 5°. Liquid droplets from such surfaces roll down at high speed, just like a solid spherical object rolling under gravity. Recreating such surfaces should consider the mechanism, by which the nature generates this property. The leaf of the lotus plants has micrometre-sized papillae covered with nanometre protrusions in the shape of branches, producing a unique hierarchical morphology (Fig. 17c) [92]. The surface chemistry is linked to epidermal cells of hydrophobic crystals. The contact area between the surface and the liquid droplet is reduced by the roughness of the hydrophobic papillae. This is the reason for liquid droplets to remain on the tips of hierarchical surface structures on top of the papillose epidermal cells. Therefore, the water-repellence nature of the lotus leaf is due to the synergy of dual-length-scale roughness and hydrophobic surface chemistry [45]. Over the years, many studies were performed to replicate the 'lotus effect' or its hydrophilic effect in industrial systems. For instance, in PEEK, improved wetting can be achieved with the utilization of high pulse frequency, low pulse overlap, and low scanning speed with a small spot size using a 1064-nm wavelength [2]. A similar effect was realized on PE and PI films upon exposure to excimer laser irradiation in air. However, the treated PE and PI became less hydrophilic with age [93].

It was established that the interactions between solids and liquids played a very important role in understanding different chemical and physical processes in various industries. Wetting is important in adhesion, but it depends on the quality of adhesive and coatings to determine spreading conditions. CA and surface free energy are employed in surface characterization to determine the wetting properties of a surface. In the laser modification of polymer films (PTFE, PET, PE, polypropylene (PP), and polystyrene (PS)) with a F_2 laser at 157-nm wavelength, laser ablation and surface degradation were noticed. Wettability, which is characterized by low CA measurements, was improved for all five polymer films. In this case, CA measurements were not only influenced by surface morphology and chemical composition but also by the number of laser pulses. Beyond 2000 pulses, CA readings remained unaltered. An abrupt increase in wettability was originally observed in PET and PE, while PTFE and PS showed a slower CA increase [93].

The two models used to describe the behaviour of a liquid droplet on a rough surface are Cassie-Baxter and

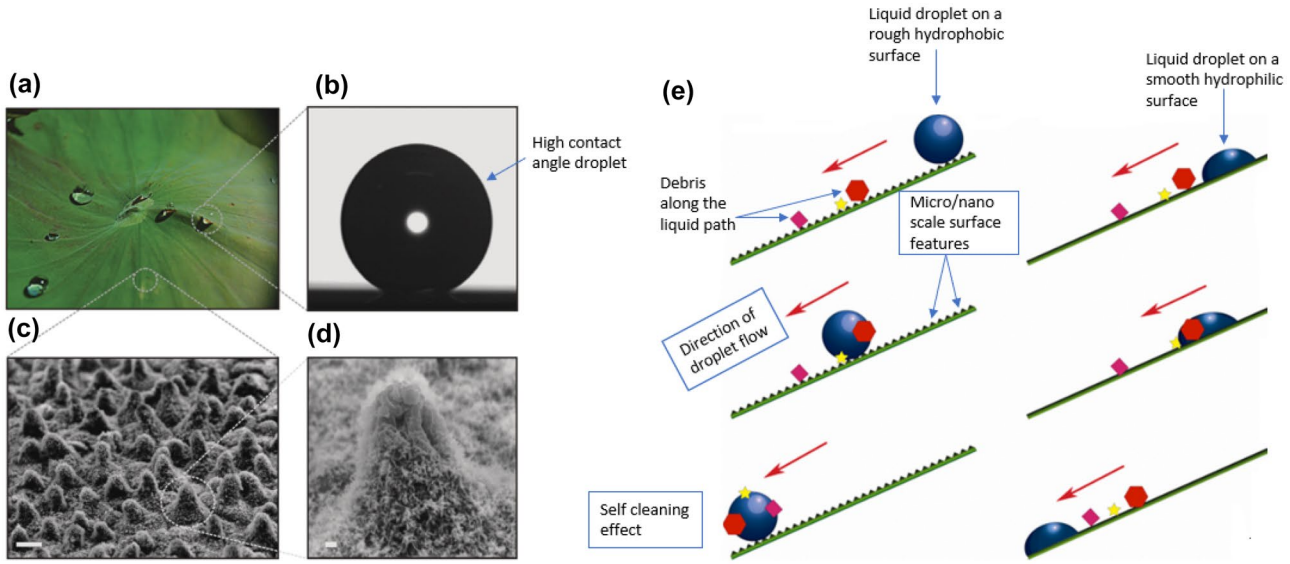

Fig. 17 **(a)** Picture of water droplets on lotus (*Nelumbo nucifera*) leaf. **(b)** Static CA measurement of a water droplet of 0.78-mm radius on the lotus leaf (CA = 153° ± 1°). **(c)** Zoomed-in SEM image of lotus leaf surface (5-μm scale bar). **(d)** SEM high-magnification micrograph of single papillose with branchlike protrusions with size of 150 nm (scale bar 1 μm) [91]. **(e)** Schematic representation of the self-cleaning mechanism of lotus leaf showing the motion of a droplet on an inclined nanostructured superhydrophobic surface covered with contaminating particles. The liquid droplet picks up debris along its path (left). In contrast, the particles on a smooth surface are only rearranged as the droplet rolls off (right) [3]

Wenzel. According to the latter, a liquid droplet has a potential to stick to a rough surface when it penetrates micro- or nano-grooves or cavities by maintaining complete contact in the process. In contrast, the former model assumes an incomplete wetting of the rough surface by the liquid droplet and trapping of air bubbles underneath the droplet in the void. The result is an air–liquid-solid composite state known as *superhydrophobic* [89, 94]. For many years, CA measurements attracted significant attention owing to technological challenges. The angle between the tangent of the solid and that of the liquid–air interface at the contact line between the three phases is referred to as the CA [95]. It is important to note that the CA is always measured through the denser fluid.

The Young's equation is valid for three-phase systems of ideal solids and pure liquids in thermodynamic equilibrium. In this case, an ideal material is smooth, isotropic, non-reactive, insoluble, and chemically homogenous. Another assumption is that evaporation does not take place, thus the volume of the liquid droplet remains unchanged.

According to Young's equation, there is a relationship between the CA θ, the surface tension of the liquid δ_L, interfacial tension (solid and liquid) δ_{SL} and the surface free energy δs of the solid (Fig. 18).

$$\delta_{SA} = \delta_{SL} + \delta_{LA}.\cos\theta_0, \tag{12}$$

$$\cos\theta_0 = \frac{SA - SL}{L} \quad . \tag{13}$$

Equation (12) applies to specific conditions and becomes modified for an inhomogeneous surface. Recalling the Wenzel model, the apparent CA is given as

$$\cos\theta = r\cos\theta_0 \tag{14}$$

where r (the roughness factor) is the ratio of the actual surface to that of an even surface with the same shape and dimensions. θ_0 is the CA on an even surface with the same properties as the rough surface. Since the roughness factor is greater than unity r > 1, this model predicts that the angle of contact increases for an initially hydrophobic

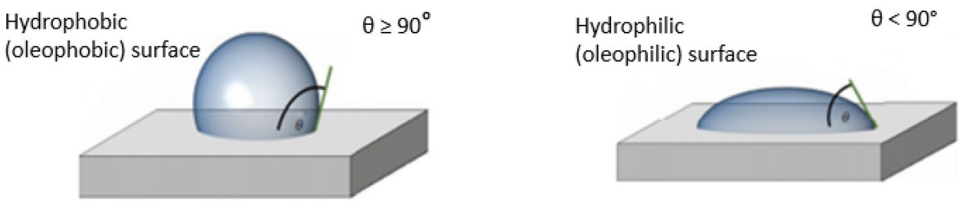

Fig. 18 Liquid drop on hydrophobic (oleophobic) and hydrophilic (oleophilic) surfaces [95]

surface $\theta_0 > 90$ and decreases for an initially hydrophilic surface $\theta_0 < 90$ [3]. A modification of the Wenzel equation incorporating a function of the wet surface and that with air pockets gives a rise to the Cassie-Baxter equation for computing CAs.

High CA values can be readily achieved on functional surfaces by the fabrication of periodic three-dimensional micro- or nano-structures by exposing the material surface to laser irradiation. In addition, the wettability nature of a textured surface may be influenced by airborne organic contaminants. Some polymeric surfaces exhibited super-hydrophilicity shortly after laser texturing but became super-hydrophobic after post-processing operations or long-term exposure to environmental contaminants [96]. This effect is significant in aged UV-laser-modified PE and PI films treated at 172-nm wavelength [93]. Therefore, it is important to ensure that laser surface treatments are carried out in controlled conditions.

5.2 Surface features and functionality

Surface structures can be classified into two categories based on the laser-patterning approach [97]: (i) direct laser-irradiated structures and (ii) self-organized laser-inscribed structures. According to the authors, directly written surface structures are complex structures written on a material surface using focused laser beams. These structures are same as those produced with the direct writing process; they include parallel or orthogonal 2D lines and complex patterns limited by the achievable spatial resolution. Self-organized characteristic (quasi-)periodic surface morphologies are produced by surface irradiation using a homogenous spatial beam profile. They are mostly nano and micro, in some cases a combination of both. Grooves and spikes in the micrometre scale and laser-induced periodic surface structures (LIPSS) or ripples all fall under this category as highlighted in Fig. 19.

Using Eq. 12, ripples can be identified as high-spatial-frequency LIPSS (Fig. 19a) with periods considerably smaller than the laser wavelength or as low-spatial-frequency LIPSS (Fig. 19b), displaying periods close to the irradiation wavelength

$$\Lambda < \lambda/2 \tag{15}$$

where Λ is the spatial period and λ is the irradiation wavelength. Ripples and grooves in Fig. 19c, d exhibit a well-marked direction with respect to the linear polarization state of the irradiation laser beam and are deformed or absent in other polarization states [3]. Previous studies showed that LIPSS were the most popular laser-induced structures in polymers. There are not many research studies that describe the fabrication of laser-induced structures on polymer materials. On the other hand, laser-inscribed surface microstructures were studied widely in metals because of a relative ease to fabricate distinct surface features on metal surfaces (Fig. 20) [31, 98].

Laser-induced periodic nano-features comprising alternate troughs and crests were observed also to impact structural colour generation on material surfaces, while hierarchical structures had a much higher potential in impacting

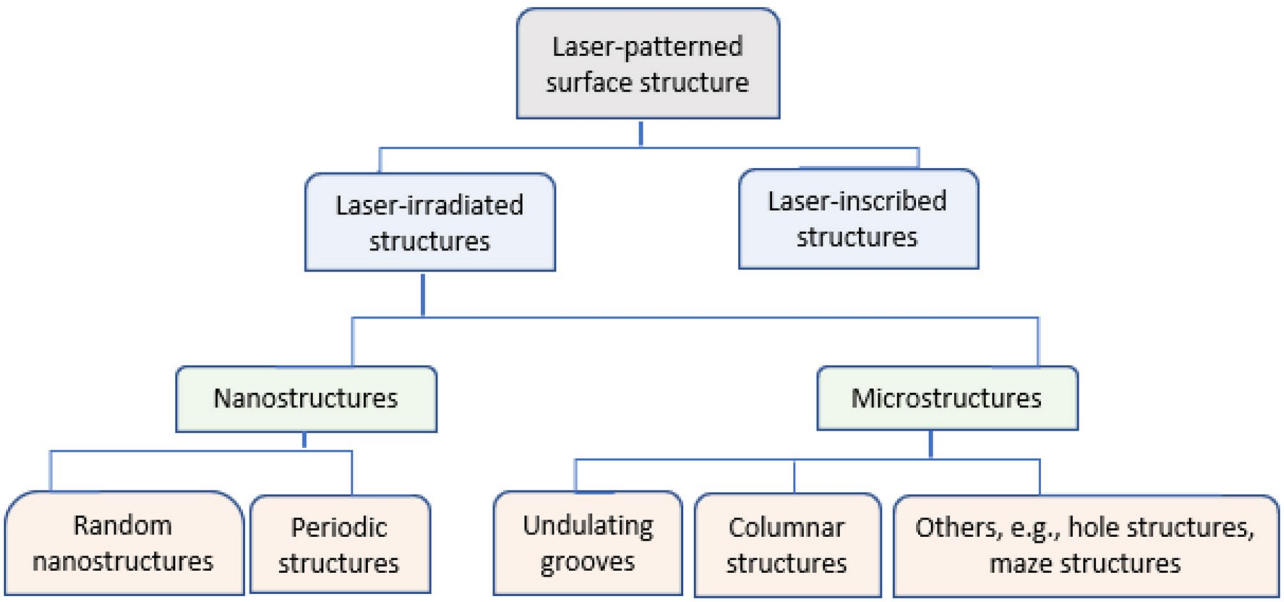

Fig. 19 Classification of laser-pattern surface structures [97]

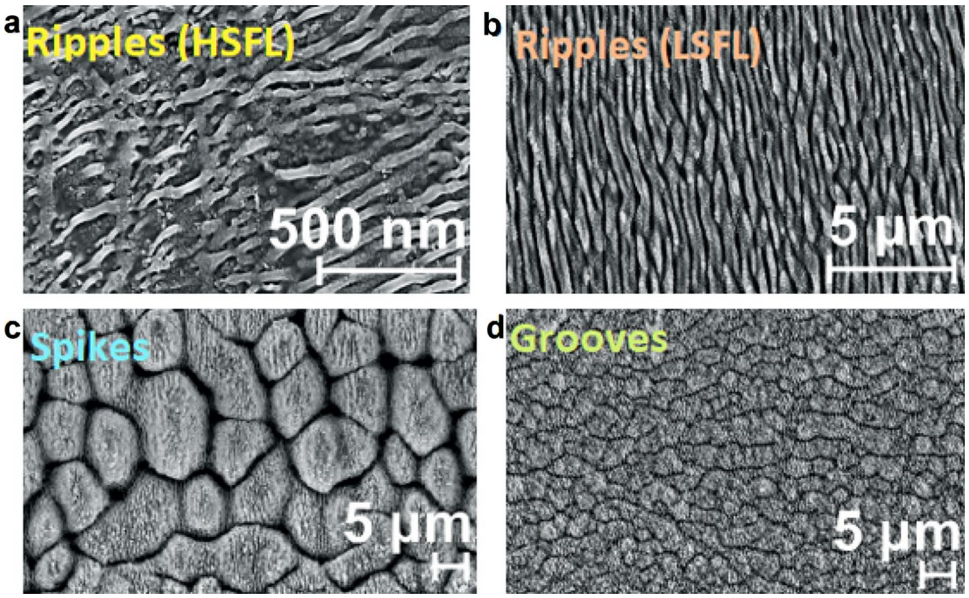

Fig. 20 SEM micrographs of four characteristic surface morphologies obtained using femtosecond laser on steel surface. **(a)** High-spatial-frequency LIPSS (HSFL). **(b)** Low-spatial-frequency LIPSS (LSFL). **(c)** Spikes. **(d)** Grooves [31]

super-hydrophobicity [31]. To explain the process of LIPSS generation, recall that high-energy laser irradiated on a material can cause its melting at the focal region. Evaporation then forces the melt to travel to the edge of the area under irradiation, forming droplets and rapid cooling, thereby forming sharp peaks on the material. The shape of the LIPSS produced is determined by the heating, recoil pressure, and solidification time, while the mechanism of patterning is a function of laser and material properties [46]. Ultrashort laser pulses (femtosecond) can produce LIPSS that are compactly covered by nanostructures. In contrast, long pulses produce LIPSS with smooth surfaces. Periodic ripples, also known as LIPSS by some authors can be created on a polymer upon irradiation at definite energy densities and for short periods. The periodic ripples formed are a product of the interference between the incident beam or refracted laser light and the diffracted beam at the material surface [35]. An increase in the angle of incidence increases the spacing between features, while the height of the ripples remains constant through the entire fluence range employed, irrespective of processing conditions. The periodic nature of ripples is a function of the polymer's surface roughness [99], and the presence of a scratch on the material surface prior to laser irradiation at different incident angles can result in the production of two sets of ripples on either side of the scratch with a spacing (S) described by the following equation [100]:

$$S = \frac{\lambda}{n - \sin\theta} \quad , \tag{16}$$

where λ is the wavelength of the incident light, n is the modified refractive index and θ is the angle of incidence. So far, there are few reports on the range of applications of the laser-irradiated structures compared to the wide range of applications offered by laser-inscribed structures [3, 97].

Although there were suggestions that hierarchically rough surfaces did not make any surface wettable, dual-scale rough surfaces display high CA values—approximately higher than 160°, with low CA hysteresis (2.5–5°). Although very low CA hysteresis is important for water repellence, high CA values obtained on textured surfaces do not determine the suitability of surface for a particular hydrophilic application [45].

In the study of surface and bulk microstructures, craters, and gratings [52] created on four different polymers, namely, polyvinyl alcohol, polystyrene, polymethyl methacrylate, and polydimethylsiloxane, surface features were achieved using 100-fs pulses of a Ti: sapphire laser at a 800-nm wavelength with a repetition rate of 1 Hz and pulse energy of 1 mJ. Results from the study showed a maximum absorption of laser energy by the materials. This absorption, which was due to transitions of different functional groups, gave a rise to emissions. The conclusion drawn from these emissions observed in the fs-laser-modified areas of different polymer surfaces indicated the possibility to create memory-based devices. Similar studies with XeCl lasers to ablate different polymers were performed by many researchers [101–103]. In some research works, the distribution of debris formed by ablation of PI and PET using XeCl and KrCl lasers was investigated [101]. Cone structures, formed on the surface of polymers, were attributed to the redeposition of debris. A different mechanism of conical structure formation was detected during the etching of PI surface using a 308-nm XeCl laser [103]. The well-defined stable conical structures formed were a result of the shielding effect of particulate impurities in the polymer film (Fig. 21).

This structure was different from those obtained on PET and PI at low fluence thresholds. The preparation of commercial film and spun-on PI samples before the experiment involved the addition of optical-grade polishes—alumina and a rare-earth compound (~ 0.05-µm and 3-µm diameters, respectively)—into liquid PI before spinning. For the commercial film, particles of the optical-grade polishes were scattered on the surface prior to irradiation. The unseeded sample (Fig. 21a) showed almost no features. The indication of a cone structure may be attributed to the presence of impurities in the material or a contamination during the sample-preparation stage. In the second micrograph (Fig. 21b), well-developed cones of different heights are observed on the substrate.

The last SEM image (Fig. 21c) of 3-µm particles shows a much higher areal density of cones. Dry etching with UV laser ablation of solid-state polymers is used for microelectronics application. Electrical and thermal insulation properties of PI result in its wide use in defence, aerospace, and optoelectronics [37]. Polydimethylsilixane (PDMS) was also broadly employed in the manufacture of microfluidic devices thanks to its transparency at optical frequencies in addition to its biocompatibility and relatively lower cost when compared to materials such as silicon formerly used in the production of such devices. Some studies [104] focused at achieving more cost-effective manufacturing approaches. One technique involved using PDMS multilayer arrangements in conventional lithography and a sputtering method to ensure alignment, while bonding the top and bottom textured substrates. In validation of the proposed technique, a dielectric photoresist-based integrated electronic microfluidic chip was produced, tested, and found to have promising potentials. Investigations on micro-contact printing and manufacture of microfluid channels using stamps on PDMS produced small features about 2 µm in pitch and a width of 1 µm [105]. Instead of the use of masks as in the photolithographic technique [106], another method involving the direct production of micro channels on PDMS was proposed and further investigated. The etching of PDMS surface using IR laser carbon materials in tiny clusters to generate micro plasma was reported in [106] to remove microscale volumes of the polymer. This method is also effective in fabricating photonic features, with the presence of combustion deposits increasing hydrophobicity.

The capability and effectiveness of using an axicon focusing lens to create narrow grooves by ablation of a thin film of molybdenum on flexible PI using a femtosecond pulsed laser was explored at different processes conditions [107]. The ablation process was carried out at various pulse energies, scanning speeds, and distances between the axicon tip and the surface of the substrate. Fairly regular groove quality and good tolerance in height fluctuations at different combinations of scribing speed and laser power were achieved. The selective scribing of molybdenum on PI was observed to be due to a notable difference in the fluence threshold of molybdenum—0.18 J/cm^2 and PI 0.75 J/cm^2 at a pulse duration of 60 fs. Generally, the ablation of several commercially available polymers was studied to understand the mechanism of material removal and possible applications of the ablated surfaces. In telecommunications, for example, removal of an outer surface of polymer materials is necessary for fibre Bragg gratings. While there are other methods to achieve this, laser ablation proved to be more efficient, eliminating the challenges encountered with traditional methods [4]. Similarly, laser ablation employed in creating tiny features on the surface of biomedical tools, devices, and implants was found beneficial in impacting their load-bearing capacity, cell and cement adhesion, wetting properties, and other features. A list of common laser textured polymers and their areas of application is presented in Table 2.

In biotechnology and medicine, in-vivo and in-vitro applications involve the adhesion of living cells to medical implants or artificial surfaces such as cell-culture substrates. Cell adhesion to substrates promotes cell growth and proliferation. For adhesion to occur, the cell skeleton is connected to the surface at focal areas. These focal areas

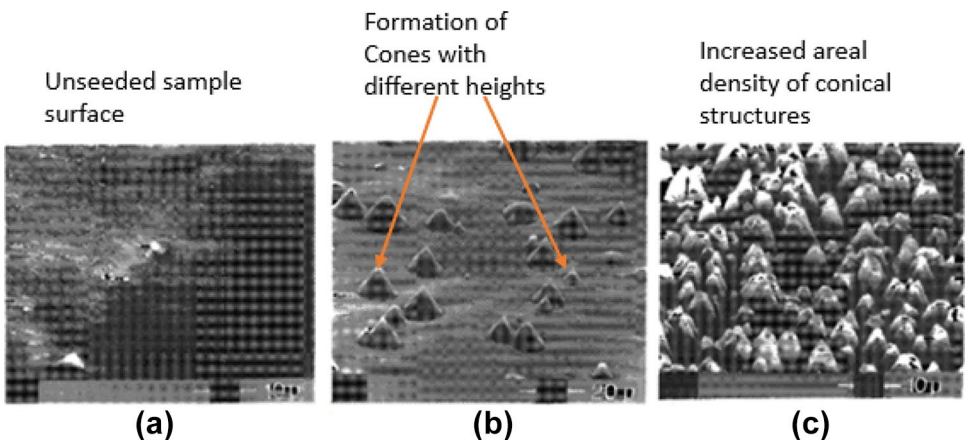

Fig. 21 SEM micrographs of XeCl-laser-etched PI (300 shots at 70 mJ/cm2). **(a)** Unseeded spun-on film. **(b)** Seeding with approximately 0.05-µm-diameter particles. **(c)** Seeding with 3-µm-diameter particles [102]

Table 2 Some laser-textured polymers and their areas of application

Laser surface textured polymers	Functionalities of textured polymers	Areas of application	References
PMMA	Unidirectional liquid transport, absorption coefficient, and thermal conductivity	Optical, biomedical, solar, sensor, and nanotechnology	[3, 4, 52, 108]
Polyvinyl alcohol	Dielectric properties	Memory-based devices	[52]
PS	Cell alignment, directional migration	Tissue engineering, cell biology, memory-based devices	[52, 109, 110]
PI	Directional fluid transport, electrical, and thermal insulation	Fluid transport against gravity, defence, aerospace, and optoelectronics	[4]
PDMS	Transparency, biocompatibility	Micro-fluidic devices, biomedicine, memory-based devices	[4, 104]
PTFE	Immobilization of living cells along required pattern, super-hydrophobicity, electrical resistance, low frictional coefficient	Tissue engineering, production of biosensors, drag reduction, cables, gears, and pulleys	[4, 111]
PET	Cell alignment, activation of β-catenin, wetting	Tissue engineering, promotion of cell proliferation, camouflage, textile industry as PE	[4, 112, 113]
Polytherimide	High-temperature resistance	Embossing tools	[4]
Polyethersulfone		Automotive components	[4, 37]
PEEK	Influence on cell growth, wettability, roughness, chemistry, adhesive bonding properties	Biomedicine	[52]
PVC	Low strength (softness)	Blood storage bags in biomedicine	[18]
PE	Reduced *E. coli biofilm* growth	Anti-bacterial surfaces	[114]
PLA	Various porosities	Bone-tissue regeneration	[115]

are influenced by factors such as surface chemistry, wettability, nano-topographies, electrostatic, and electrodynamic charges [116–119].

Many polymeric biomaterials were studied for tissue-engineering applications, e.g., PEEK. PEEK is an engineering thermoplastic that exhibits excellent mechanical properties and good thermal and chemical resistance, which are similar to those of cortical bone [120]. In addition to these properties, the sterilization capacity of PEEK makes it an ideal material for most biomedical applications [121]. PEEK is used in joint replacement, bone screws and pins (e.g., in the vertebra column), cranial implants, etc. Despite these attractive properties, the poor surface wettability of PEEK makes weak bone-to-implant interactions.

Initial studies on the LST of PEEK were carried out using excimer lasers [122] in the presence of an assist gas. Argon fluoride (Arf) lasers with a wavelength of 193 nm and 20 ns pulse duration modified PEEK surfaces below the ablation threshold, increasing the polar component of the work of adhesion. Experimental findings showed that, in neutral conditions, PEEK aromaticity was lost, and the present carbonyl groups were broken. High energetic incident photons improved C–O/C and carboxylic functions of PEEK in the presence of environmental oxygen. Laser processing of PEEK surface at 1064 nm using a Q-switched Nd:YAG laser improved the surface together with an increase in the surface energy from 44.9 to 78 mJ/m^2. Further chemical surface analysis using FTIR and XPS showed a decrease in the carbonyl groups along with an increase in carboxylic and hydroxyl groups [123]. From several studies, surface functionalization of PEEK with LST was most successful with wavelengths in the range of UV (355 nm) to mid-infrared (10.6 µm) [2, 123, 124]. UV-laser modification of PEEK at 248 nm wavelength demonstrated the wettability with increased roughness and oxygen-containing groups on the processed-material surface [125]. In the study performed to compare the influence of wavelength on wettability and roughness, three different laser wavelengths within the UV and mid-infrared range were used. The response of PEEK at different wavelengths was observed to differ. Surface burning was prevalent at 1064-nm laser wavelength, while ablation took place at 532 nm, resulting in the formation of grooves about 100 µm in average width. Minor surface melting occurred at 355 nm, inducing the formation of carboxyl and peroxide (O–O) polar groups. This led to a noticeable reduction in the water CA. Reduced surface wettability of PEEK can potentially improve cell adhesion, which is ideal for biomedical applications [87]. Table 3 summarizes process parameters applied in the texturing and surface modification of PEEK for biomedical applications.

Although some works were performed on LST of polymers for tribological applications, polymers are rarely the material of choice in this area. Generally, the presence of artificial textures showed to improve wear performance of

Table 3 Summary of processing parameters from selected works on LST of PEEK and PEEK plus nano particles of SiO_2 (marked as *) for biomedical applications

Material	Thickness/ form	Laser/mode	Wavelength (nm)	Power (W)	Spot diameter (µm)	Fluence (J/ cm^2)	Focal length (mm)	Freq. (KHz)	Pulse duration	Pulse number	Technique	Feature	Scan speed (mm/s)	Ra (µm)/ WCA (°)	Application	Ref
PEEK	250 µm (film)	ArF excimer/P	193	-	-	$5–80 \times 10^{-3}$	-	0.01	20 ns	1–2000	Stationary beam	Conical structures	-		Influence on adhesive bonding properties	[127]
	8 mm (plate)	Nd:YVO_4/P	1064	5–39	100–1000	-	211	15.2–50	~ns	-	GS	PS	200–5000	≥ 1	Increased roughness and wettability (biomedical)	[87]
	8 mm (plate)	Nd:YVO_4/P	532	5–39	100–1000	-	365	15.2–50	~ns	-	GS	PG	200–5000	≥ 1	Increased roughness and wettability (biomedical)	[87]
	8 mm (plate)	Nd:YVO_4/P	355	5–39	100–1000	-	235	15.2–50	~ns	-	GS	PG	200–5000	< 1 µm	Increased roughness and wettability (biomedical)	[87]
	-	Nd:YAG/P	355	-	450	0.75	-	-	38 ns	4–12	Interference patterning	Line structures	-		Influence on cell growth (biomedical)	[128]
	-	ArF excimer/P	193	-	-	3.5	-	-	20–25 ns	10	Stationary beam + mask	PG	-		Influence on pre-osteoblastic cell response (biomedical)	[129]
	240 µm membranes	CO_2/quasi-CW	10,600	1	-	-	100	5	~ms	-	GS	PG	-		Influence on osteoblast response (biomedical)	[130]
	3.92-mm (coupon)	Q-switched Nd:YAG/P	1064	-	600–2500	0.01–0.1	-	0.01	10 ns	-	XY sample stage	Dimples	12	NA/25	Influence on adhesive bonding properties	[123]
	50 µm (foil)	KrF excimer/P	248	-	-	0.004–0.03	-	0.01	20–40 ns	6000	XY sample stage	Ripples and dots	-	17×10^{-3}/50	Influence on roughness chemistry, cell adhesion, and wettability (biomedical)	[131]

Table 3 (Continued)

Material	Thickness/ form	Laser/mode	Wavelength (nm)	Power (W)	Spot diameter (µm)	Fluence (J/ cm^2)	Focal length (mm)	Freq. (KHz)	Pulse duration	Pulse number	Technique	Feature	Scan speed (mm/s)	Ra (µm)/ WCA (°)	Application	Ref
	2 mm (sheet)	Ti:sapphire/P	800	0.02	-	-	-	1.0	-	-	-	PG	1	0.6245/54.8	Influence on osteogenic response (biomedical)	[132]
*	2 mm (sheet)	Ti:sapphire/P	800	0.02	-	-	-	1.0	-	-	-	PG	1		Influence on osteogenic response (biomedical)	[132]

P pulsed, *PG* parallel grooves, *GS* galvanometric scanning system

kinematic pairs. Friction reduction with an increase in wear resistance was the focus of many studies. Several works established that surface textures could serve as storage pockets for lubricants, depending on texture design and pattern. Ultimately, the influence of texture shapes in tribology is relatively complex to study since shapes and aspect ratios of textures as well as the textured area should be similar for comparative and robust analysis [126]. Hence, the influence of surface textures on surface properties presented in this section is related to biomedical applications. A proper analysis of the effect of textures on wettability was discussed in depth. Since PEEK is one of the biopolymers with good properties, attention was on it and a table of process parameters for LST of PEEK was also included. In all, many studies were done on LST of different polymers. Some challenges discussed in this review are highlighted in the next section with suggestions for future directions. These concerns should be addressed in future works to benefit both research and industrial purposes.

6 Challenges and future directions

There is no doubt that significant scientific achievements have been made in laser-beam micromachining of polymers; however, this research field is still developing. Many works made a good attempt to present process parameters and chemical modifications leading to improved surface functionality in certain polymers. However, the contribution of topography and the exact features that are responsible for various functionalities are still unclear. This makes it especially challenging for industrial settings where reproducibility is crucial. Secondly, the reviewed studies show that polymers adopted for laser-ablation research are selected based on categories such as availability, ablation mechanism, applications, decomposition behaviour, and cost. More research is needed on a wider variety of polymers with the aim of identifying novel potential applications in different promising fields.

Ultrashort-pulse laser machining with DLIP was found to be a remarkable technique for creating a variety of surface features down to the nanometre scale, a feat difficult to achieve with other texturing techniques. However, few works were done on DLIP of polymers, and these were carried out mostly using a two-beam interference configuration. Therefore, more research is needed on more polymers using different numbers of interfering laser beams for a more robust analysis of the suitability of this technique. Although the complexity in setting up the optics to achieve an interference pattern poses a major challenge (as reported in previous studies), more research should be encouraged. The development and configuration of DLIP systems that allow the interference of multiple laser beams can lead to

full exploration of the capabilities and potentials of the DLIP technique. Other aspects that can be improved are the processing speed and the achievable feature size. While this was largely improved by the DLIP technique, more research can explore the possibility of achieving novel surface features and sizes that enhance surface functionality with a shorter processing time. For easy implementation on the industrial scale, a digital compilation and modelling of optimal process parameters with corresponding texture geometries for different polymeric materials should be developed. Specific environmental/service conditions that influence certain surface functionalities could also be incorporated in a software design for high-repetition-rate femtosecond lasers. The idea is to improve precision, accuracy, process control, and reproducibility of texture designs and potentially increase the fabrication rate from a manufacturing point of view.

7 Conclusions

In this review, common surface modification methods for polymers are discussed with a focus on the mechanism responsible for altering the surface morphology, texture geometry, and surface properties, which affect functionality. Studies reveal that several texturing techniques have been explored with a view to; investigate polymer's response to process parameters, produce a functional surface, and establish efficacy of a technique or a comparison between techniques. In some works, more than one surface treatment process was explored on pure polymers and/or polymer composites. All the techniques reported in this work have advantages and shortcomings. The choice of processing technique to be adopted by a researcher is dependent on several factors. Therefore, it is important to have in-depth knowledge of the different micro-texturing techniques to identify a suitable one for a required outcome. Ultra-fast laser texturing is proved to be a viable surface modification technology. Also, the exploration of different laser beam delivery methods provides some flexibility in the texturing process since feature size and geometry and be controlled to produce novel features.

In general, this review has provided a summary of the studies carried out on ultra-fast laser micro/nano texturing of different polymers within the past two decades. The potential of the LST by DLIP to tailor the biological performance of biopolymers that are currently being used in clinical practice was also demonstrated. In addition, it aims to provide a foundation for exploring various laser surface modification methods and serves as a guide for other researchers and scientists involved in laser texturing (micro and nano) of polymers.

Author contribution All authors contributed significantly to the work with the order provided.

Funding This publication was made possible by the sponsorship and support of Loughborough University. The work was enabled through, and undertaken at, the National Structural Integrity Research Centre (NSIRC), a postgraduate engineering facility for industry-led research into structural integrity established and managed by TWI through a network of both national and international Universities.

Availability of data and materials The authors confirm that the data and material supporting the findings of this work are available within the article.

Code availability Not applicable.

Declarations

Ethics approval Not applicable.

Consent to participate Informed consent was obtained from all individual participants included in this study.

Consent for publication All individual participants declare that they accept to submit this paper for publication.

Conflict of interest The authors declare no competing interests.

References

1. Prakash CGJ, Prasanth R (2021) Approaches to design a surface with tunable wettability: a review on surface properties. J Mater Sci 56(1):108–135. https://doi.org/10.1007/s10853-020-05116-1
2. Riveiro A, Maçon ALB, del Val J, Comesaña R, Pou J (2018) Laser surface texturing of polymers for biomedical applications. Frontiers Media S.A. Front Phys 5. https://doi.org/10.3389/fphy.2018.00016
3. Stratakis E et al (2020) Laser engineering of biomimetic surfaces. Elsevier Ltd. AR: Reports Mater Sci Eng 141. https://doi.org/10.1016/j.mser.2020.100562
4. Ravi-Kumar S, Lies B, Zhang X, Lyu H, Qin H (2019) Laser ablation of polymers: a review. John Wiley and Sons Ltd. Polym Int 68(8):1391–1401. https://doi.org/10.1002/pi.5834
5. Verma S, Sharma N, Kango S, Sharma S (2021) Developments of PEEK (Polyetheretherketone) as a biomedical material: a focused review. Eur Polym J 147(2020):1–10. https://doi.org/10.1016/j.eurpolymj.2021.110295
6. Shen MX, Zhang ZX, Yang JT, Yao Xiong G (2019) Wetting behavior and tribological properties of polymer brushes on laser-textured surface. Polymers (Basel) 11(6). https://doi.org/10.3390/polym11060981

7. Deshmukh SS, Goswami A (2019) Hot embossing of polymers - a review. Mater Today Proc 26:405–414. https://doi.org/10.1016/j.matpr.2019.12.067
8. Hamilton D, Ghrebi S, Kim H, Chehroudi B, Brunette D (2008) Surface topography and cell behavior. Encycl Biomater Biomed Eng Second Ed 4:2551–2561. https://doi.org/10.1201/b18990-246
9. Ruszaj A, Cygnar M, Grabowski M (2018) The state of the art in electrochemical machining process modeling and applications. AIP Conf Proc 2017. https://doi.org/10.1063/1.5056292
10. Rajput NS, Luo X (2015) FIB Micro/Nano-fabrication, Second Edi. Yi Qin
11. Zanjani MY, Hackert-Oschätzchen M, Martin A, Meichsner G, Edelmann J, Schubert A (2019) Process control in jet electrochemical machining of stainless steel through inline metrology of current density. Micromachines 10(4). https://doi.org/10.3390/mi10040261
12. Yilbas BS, Al-Sharafi A, Ali H (2019) Surfaces for Self-Cleaning
13. Kim CS, Ahn SH, Jang DY (2012) Review: developments in micro/nanoscale fabrication by focused ion beams. Vacuum 86(8):1014–1035. https://doi.org/10.1016/j.vacuum.2011.11.004
14. Patil D, Sharma A, Aravindan S, Rao PV (2019) Development of hot embossing setup and fabrication of ordered nanostructures on large area of polymer surface for antibiofouling application. Micro Nano Lett 14(2):191-5. https://doi.org/10.1049/mnl.2018.5462.
15. McCrum CBBNG, Buckley CP, Clive B (1997) Bucknall, Principles of polymer engineering. Oxford: Oxford Science publications
16. Hanafy TA, Nouh SA, Yasein MN, El Sayed AM (2012) Influence of laser irradiation on the optical and the mechanical properties of Makrofol-DE polycarbonate. J Appl Polym Sci 124(6):4620–4627. https://doi.org/10.1002/app.35548
17. Hossain S (2019) Optical properties of polymers and their applications. [Online]. Available: https://digitalcommons.njit.edu/theses/1685
18. Mustafa NS, Omer MA, Garlnabi ME, Ismail HA, Ch CH (2016) Reviewing of general polymer types, properties and application in medical field. Int J Sci Res (IJSR) 5(8):212e221. https://doi.org/10.21275/art2016772
19. Pham D et al (2002) Effects of polymer properties on laser ablation behaviour. Smart Mater Struct 11(5):668–674. https://doi.org/10.1088/0964-1726/11/5/307
20. Kantesh Balani RN, Verma V, Agarwal A (2014) Physical, thermal, and mechanical properties of polymers A1.1 physical properties
21. T'Joen C, Park Y, Wang Q, Sommers A, Han X, Jacobi A (2009) A review on polymer heat exchangers for HVAC&R applications. Int J Refrig 32(5):763–779. https://doi.org/10.1016/j.ijrefrig.2008.11.008
22. Reay D (1989) The use of polymers in heat exchangers. HRV
23. Deronzier G, Bertolini JC (1997) Plate heat exchanger in liquid crystal polymer. Appl Therm Eng 17:799–808
24. Wharry SR Jr (2002) Fluoropolymer heat exchangers. Met Finish 100:752–762
25. Gupta MK, Srivastava RK, Bisaria H, Gupta MK, Srivastava RK (2015) Potential of jute fibre reinforced polymer composites: a review green composite prepared by waste sugarcane bagasse and poly lactic acid (PLA) for packaging application view project machining of superalloys and smart materials. J Int J Fiber Text Res 5(3):30–38. [Online]. Available: http://www.urpjournals.com
26. Gamaly EG (2011) The physics of ultra-short laser interaction with solids at non-relativistic intensities. Phys Rep 508(4–5):91–243. https://doi.org/10.1016/j.physrep.2011.07.002
27. del Cerro DA (2014) Picosecond pules laser microstructuring of metals for microfluidics. PhD Thesis 1–166
28. Pacella M (2014) Pulsed laser ablation (PLA) of ultra-hard structures: generation of damage-tolerant freeform surfaces for advanced machining applications
29. Stepak B, Antończak AJ, Bartkowiak-Jowsa M, Filipiak J, Pezowicz C, Abramski KM (2014) Fabrication of a polymer-based biodegradable stent using a CO2 laser. Arch Civ Mech Eng 14(2):317–326. https://doi.org/10.1016/j.acme.2013.08.005
30. Mishra S, Yadava V (2015) Laser beam micromachining (LBMM) - a review. Elsevier Ltd. Opt Lasers Eng 73:89–122. https://doi.org/10.1016/j.optlaseng.2015.03.017
31. Assaf Y, Kietzig AM (2018) Optical and chemical effects governing femtosecond laser-induced structure formation on polymer surfaces. Mater Today Commun 14(January):169–179. https://doi.org/10.1016/j.mtcomm.2018.01.008
32. Singh A, Patel DS, Ramkumar J, Balani K (2019) Single step laser surface texturing for enhancing contact angle and tribological properties. Int J Adv Manuf Technol 100(5–8):1253–1267. https://doi.org/10.1007/s00170-018-1579-8
33. Petrović V, Delibašić H (2019) "Improved treatment of the photoionization process in the laser induced optical breakdown in the laser tissue", *UPB Sci*. Bull Ser A Appl Math Phys 81(4):287–300
34. Liu X, Du D, Mourou G (1997) Laser ablation and micromachining with ultrashort laser pulses
35. Nemani SK et al (2018) Surface modification: surface modification of polymers: methods and applications. Adv Mater Interfaces 5(24):1870121. https://doi.org/10.1002/admi.201870121
36. Garrison BJ, Srinivasan R (1985) Laser ablation of organic polymers: microscopic models for photochemical and thermal processes. J Appl Phys 57(8):2909–2914. https://doi.org/10.1063/1.335230
37. Ravi-Kumar S, Lies B, Lyu H, Qin H (2019) Laser ablation of polymers: a review. Procedia Manufacturing 34:316–327. https://doi.org/10.1016/j.promfg.2019.06.155
38. Jaeggi B, Neuenschwander B, Schmid M, Muralt M, Zuercher J, Hunziker U (2011) Influence of the pulse duration in the ps-regime on the ablation efficiency of metals. Physics Procedia (12)2:164 171. https://doi.org/10.1016/j.phpro.2011.03.118
39. Wood MJ, Coady MJ, Aristizabal F, Nielsen K, Ragogna PJ, Kietzig AM (2019) Femtosecond laser micromachining of co-polymeric urethane materials. Appl Surf Sci 483:633–641. https://doi.org/10.1016/j.apsusc.2019.03.296
40. Baudach S, Krüger J, Kautek W (2001) Femtosecond laser processing of soft materials. Rev Laser Eng 29(11):705–709. https://doi.org/10.2184/lsj.29.705
41. Guay JM, Villafranca A, Baset F, Popov K, Ramunno L, Bhardwaj VR (2012) Polarization-dependent femtosecond laser ablation of poly-methyl methacrylate. New J Phys 14. https://doi.org/10.1088/1367-2630/14/8/085010
42. Baudach S, Bonse J, Krüger J, Kautek W (2000) Ultrashort pulse laser ablation of polycarbonate and polymethylmethacrylate. https://doi.org/10.1016/S0169-4332(99)00474-2
43. Zhang Q et al (2020) Laser-induced wettability gradient surface on NiTi alloy for improved hemocompatibility and flow resistance. Mater Sci Eng C 111:110847. https://doi.org/10.1016/j.msec.2020.110847
44. David Phillips S, Simpson S (2017) Optomechanical microtools and shape-induced forces
45. Zorba V et al (2008) Biomimetic artificial surfaces quantitatively reproduce the water repellency of a lotus leaf. Adv Mater 20(21):4049–4054. https://doi.org/10.1002/adma.200800651
46. Martínez-Calderon M et al (2016) Surface micro- and nano-texturing of stainless steel by femtosecond laser for the control

of cell migration. Sci Rep 6(July):1–10. https://doi.org/10.1038/srep36296
47. Wang X, Li C, Hong W, Ma C, Xing Y, Feng J (2018) Fabrication of ordered hierarchical structures on stainless steel by picosecond laser for modified wettability applications. Opt Express 26(15):18998. https://doi.org/10.1364/oe.26.018998
48. Skoulas E, Manousaki A, Fotakis C, Stratakis E (2017) Biomimetic surface structuring using cylindrical vector femtosecond laser beams. Sci Rep 7. https://doi.org/10.1038/srep45114
49. Wang R, Wei J, Fan Y (2014) Chalcogenide phase-change thin films used as grayscale photolithography materials. Opt Express 22(5):4973. https://doi.org/10.1364/oe.22.004973
50. Kulander K, Lewenstein M (2006) Multiphoton and strong-field processes. Springer Handbook of Atomic 1077. https://doi.org/10.1007/978-0-387-26308-3_74
51. Ou Y et al (2015) Direct fabrication of microlens arrays on PMMA with laser-induced structural modification. IEEE Photonics Technol Lett 27(21):2253–2256. https://doi.org/10.1109/LPT.2015.2459045
52. Kallepalli LND (2012) Femtosecond-laser direct writing in polymers and potential applications in microfluidics and memory devices. Opt Eng 51(7):073402. https://doi.org/10.1117/1.oe.51.7.073402
53. Lang V, Roch T, Lasagni AF (2016) High-speed surface structuring of polycarbonate using direct laser interference patterning: toward 1 m2 min−1 fabrication speed barrier. Adv Eng Mater 18(8):1342–1348. https://doi.org/10.1002/adem.201600173
54. Milles S, Voisiat B, Nitschke M, Lasagni AF (2019) Influence of roughness achieved by periodic structures on the wettability of aluminum using direct laser writing and direct laser interference patterning technology. J Mater Process Technol 270(January):142–151. https://doi.org/10.1016/j.jmatprotec.2019.02.023
55. Voisiat B, Aguilar-Morales AI, Kunze T, Lasagni AF (2020) Development of an analytical model for optimization of direct laser interference patterning. Materials 13(1). https://doi.org/10.3390/ma13010200
56. Alamri S, Lasagni AF (2017) Development of a general model for direct laser interference patterning of polymers. Opt Express 25(9):9603. https://doi.org/10.1364/oe.25.009603
57. Stankevičius E, Malinauskas M, Gedvilas M, Voisiat B, Račiukaitis G (2011) Fabrication of periodic micro-structures by multi-photon polymerization using the femtosecond laser and four-beam interference. Medziagotyra 17(3):244–248. https://doi.org/10.5755/j01.ms.17.3.587
58. Nemani K, Annavarapu RK, Raiyan A (2018) Surface modification : surface modification of polymers : methods and surface modification of polymers : methods and applications. https://doi.org/10.1002/admi.201801247
59. Lasagni A, Manzoni A, Mücklich F (2007) Micro/nano fabrication of periodic hierarchical structures by multi-pulsed laser interference structuring. Adv Eng Mater 9(10):872–875. https://doi.org/10.1002/adem.200700176
60. Zhai T, Zhang X, Pang Z, Dou F (2011) Direct writing of polymer lasers using interference ablation. Adv Mater 23(16):1860–1864. https://doi.org/10.1002/adma.201100250
61. Delaporte IZP, Karnakis D (2015) Handbook of flexible organic electronics; material, manufacturing and applications. Woodhead publishing
62. Bieda M, Siebold M, Lasagni AF (2016) Fabrication of submicron surface structures on copper, stainless steel and titanium using picosecond laser interference patterning. Appl Surf Sci 387:175–182. https://doi.org/10.1016/j.apsusc.2016.06.100
63. Aguilar-Morales AI, Alamri S, Lasagni AF (2018) Micro-fabrication of high aspect ratio periodic structures on stainless steel by picosecond direct laser interference patterning. J Mater Process Technol 252:313–321. https://doi.org/10.1016/j.jmatprotec.2017.09.039
64. Voisiat B, Aguilar-Morales AI, Kunze T, Lasagni AF (2020) Development of an analytical model for optimization of direct laser interference patterning. Materials (Basel) 13(1):1–10. https://doi.org/10.3390/ma13010200
65. Nakata Y, Yoshida M, Osawa K, Miyanaga N (2017) Fabricating a regular hexagonal lattice structure by interference pattern of six femtosecond laser beams. Appl Surf Sci 417:69–72. https://doi.org/10.1016/j.apsusc.2017.03.236
66. Indrisiunas S, Voisiat B, Žukauskas A, Račiukaitis G (2015) Direct laser beam interference patterning technique for fast high aspect ratio surface structuring. Laser Appl Microelectron Optoelectron Manuf 9350:935003. https://doi.org/10.1117/12.2079826
67. Lasagni AF, Acevedo DF, Barbero CA, Mücklich F (2008) Direct patterning of polystyrene-polymethyl methacrylate copolymer by means of laser interference lithography using UV laser irradiation. Polym Eng Sci 48(12):2367–2372. https://doi.org/10.1002/pen.21189
68. Mitra A, Thareja RK (1999) Determination of laser ablation threshold of Teflon at different harmonics of Nd:YAG laser using photothermal deflection technique. https://doi.org/10.1023/A:1004567301546
69. Paschotta R (2008) Field guide to laser pulse generation. Rudiger P. SPIE Press. Bellingham, WA, pp 23–26
70. Kuper S, Stuke M (1987) Alzglied physics Physics B, n. Laser Femtosecond uv Excimer Laser Ablation
71. Huber N, Heitz J, Bäuerle D (2004) Pulsed-laser ablation of polytetrafluoroethylene (PTFE) at various wavelengths. EPJ Appl Phys 33–38
72. Brannon JH, Lankard JR, Baise AI, Burns F, Kaufman J (1985) Excimer laser etching of polyimide. J Appl Phys 58(5):2036–2043. https://doi.org/10.1063/1.336012
73. Taylor RS, Singleton DL, Paraskevopoulos G (1987) Effect of optical pulse duration on the XeCl laser ablation of polymers and biological tissue. Appl Phys Lett 50(25):1779–1781. https://doi.org/10.1063/1.97744
74. Chuang MC, Tam AC (1989) On the saturation effect in the picosecond near ultraviolet laser ablation of polyimide. J Appl Phys 65(7):2591–2595. https://doi.org/10.1063/1.342788
75. Wang ZB, Hong MH, Lu YF, Wu DJ, Lan B, Chong TC (2003) Femtosecond laser ablation of polytetrafluoroethylene (Teflon) in ambient air. Int J Appl Phys 93(10):6375-80. https://doi.org/10.1063/1.1568154
76. Liu X, Du D, Mourou G (1997) Laser ablation and micromachining with ultrashort laser pulses. IEEE J Quantum Electron 33(10):1706–1716. https://doi.org/10.1109/3.631270
77. Bauerle D (2011) Laser processing and chemistry
78. He C, Steger M, Gillner A (2018) High-efficiency nanostructuring using multi-beam interference by consecutively deposited ultrashort laser pulses on tool steel. J Laser Micro Nanoeng 13(1):1–5. https://doi.org/10.2961/jlmn.2018.01.0001
79. Aguilar-Morales AI, Alamri S, Kunze T, Lasagni AF (2018) Influence of processing parameters on surface texture homogeneity using direct laser interference patterning. Opt Laser Technol 107:216–227. https://doi.org/10.1016/j.optlastec.2018.05.044
80. Soldera M, Alamri S, Storm S, Kunze T, Lasagni AF (2020) Maximizing the efficiency of laser-fabricated diffraction gratings on PET using direct laser interference patterning p. 34. https://doi.org/10.1117/12.2543736
81. Rodriguez A et al (2009) Laser interference lithography for nanoscale structuring of materials: From laboratory to industry.

Microelectron Eng 86(4–6):937–940. https://doi.org/10.1016/j.mee.2008.12.043
82. D'alessandria M, Lasagni A, Mücklich F (2008) Direct micropatterning of aluminum substrates via laser interference metallurgy. Applied surface science 255:3210–3216. https://doi.org/10.1016/j.apsusc.2008.09.018
83. Lutey AHA (2013) An improved model for nanosecond pulsed laser ablation of metals. J Appl Phys 114(8). https://doi.org/10.1063/1.4818513
84. Akkan CK et al (2013) Plasma and short pulse laser treatment of medical grade PEEK surfaces for controlled wetting. Mater Lett 109:261–264. https://doi.org/10.1016/j.matlet.2013.07.030
85. Oliveira V, Nunes B, Vilar R (2010) Wetting response of KrF laser ablated polyimide surfaces. Nucl Inst Methods Phys Res B 268:1626–1630. https://doi.org/10.1016/j.nimb.2010.03.006
86. Yong J et al (2018) Femtosecond laser direct writing of porous network microstructures for fabricating super-slippery surfaces with excellent liquid repellence and anti-cell proliferation. Adv Mater Interfaces 5(7). https://doi.org/10.1002/admi.201701479
87. Riveiro A et al (2012) Laser surface modification of PEEK. Appl Surf Sci 258(23):9437–9442. https://doi.org/10.1016/j.apsusc.2012.01.154
88. Hussain M et al (2020) Polymers ultra-high-molecular-weight-polyethylene (UHMWPE) as a promising polymer material for biomedical applications: a concise review. https://doi.org/10.3390/polym12020323
89. Cai Y, Lin L, Xue Z, Liu M, Wang S, Jiang L (2014) Filefish-inspired surface design for anisotropic underwater oleophobicity. Adv Funct Mater 24(6):809–816. https://doi.org/10.1002/adfm.201302034
90. Liang F, Lehr J, Danielczak L, Leask R, Kietzig AM (2014) Robust non-wetting PTFE surfaces by femtosecond laser machining. Int J Mol Sci 15(8):13681–13696. https://doi.org/10.3390/ijms150813681
91. Stratakis E, Ranella A, Fotakis C (2011) Biomimetic micro/nanostructured functional surfaces for microfluidic and tissue engineering applications. Biomicrofluidics 5(1). https://doi.org/10.1063/1.3553235
92. Rafael R, Gattass, Mazur E (2008) Femto second laser micro machining in transparent materials. Nat Photonics
93. Rodríguez E et al (1989) We are IntechOpen, the world's leading publisher of Open Access books Built by scientists, for scientists TOP 1 %. Intech 32:137–144. Available: https://www.intechopen.com/books/advanced-biometric-technologies/liveness-detection-in-biometrics
94. Toosi SF, Moradi S, Ebrahimi M, Hatzikiriakos SG (2016) Microfabrication of polymeric surfaces with extreme wettability using hot embossing. Appl Surf Sci 378:426–434. https://doi.org/10.1016/j.apsusc.2016.03.116
95. Marmur A, Della Volpe C, Siboni S, Amirfazli A, Drelich JW (2017) Contact angles and wettability: towards common and accurate terminology. Surf Innov 5(1):3–8. https://doi.org/10.1680/jsuin.17.00002
96. Samanta A, Wang Q, Shaw SK, Ding H (2020) Roles of chemistry modification for laser textured metal alloys to achieve extreme surface wetting behaviors. Mater Des p. 108744. https://doi.org/10.1016/j.matdes.2020.108744
97. Tanvir Ahmmed KM, Grambow C, Kietzig AM (2014) Fabrication of micro/nano structures on metals by femtosecond laser micromachining. Micromachines 5(4):1219–1253. https://doi.org/10.3390/mi5041219
98. Ijaola AO et al (2020) Wettability transition for laser textured surfaces: a comprehensive review. Surf Interfaces 21:100802. https://doi.org/10.1016/j.surfin.2020.100802
99. Borowiec A, Haugen HK (2003) Subwavelength ripple formation on the surfaces of compound semiconductors irradiated with femtosecond laser pulses. Appl Phys Lett 82(25):4462–4464. https://doi.org/10.1063/1.1586457
100. Barberoglou M, Gray D, Magoulakis E, Fotakis C, Loukakos PA, Stratakis E (2013) Controlling ripples' periodicity using temporally delayed femtosecond laser double pulses. Opt Express 21(15):18501. https://doi.org/10.1364/oe.21.018501
101. Taylor RS, Leopold KE, Singleton DL, Paraskevopoulos G, Irwin RS (1988) The effect of debris formation on the morphology of excimer laser ablated polymers. J Appl Phys 64(5):2815–2818. https://doi.org/10.1063/1.341590
102. Dyer PE, Jenkins SD, Sidhu J (1986) Development and origin of conical structures on XeCl laser ablated polyimide. Appl Phys Lett 49(8):453–455. https://doi.org/10.1063/1.97113
103. Niino H, Shimoyama M, Yabe A (1990) XeCl excimer laser ablation of a polyethersulfone film: dependence of periodic microstructures on a polarized beam. Appl Phys Lett 57(22):2368–2370. https://doi.org/10.1063/1.103873
104. Li M, Li S, Wu J, Wen W, Li W, Alici G (2012) A simple and cost-effective method for fabrication of integrated electronic-microfluidic devices using a laser-patterned PDMS layer. Microfluid Nanofluidics 12(5):751–760. https://doi.org/10.1007/s10404-011-0917-z
105. Wolfe DB, Ashcom JB, Hwang JC, Schaffer CB, Mazur E, Whitesides GM (2003) Customization of poly(dimethylsiloxane) stamps by micromachining using a femtosecond-pulsed laser. Adv Mater 15(1):62–65. https://doi.org/10.1002/adma.200390012
106. Hsieh YK et al (2017) Direct micromachining of microfluidic channels on biodegradable materials using laser ablation. Polymers (Basel) 9(7). https://doi.org/10.3390/polym9070242
107. Yu X, Ma J, Lei S (2015) Femtosecond laser scribing of Mo thin film on flexible substrate using axicon focused beam. J Manuf Process 20:349–355. https://doi.org/10.1016/j.jmapro.2015.05.004
108. Chen H, Zhang L, Zhang Y, Zhang P, Zhang D, Jiang L (2017) Uni-directional liquid spreading control on a bio-inspired surface from the peristome of Nepenthes alata. J Mater Chem A 5(15):6914–6920. https://doi.org/10.1039/c7ta01609c
109. Jin CY, Zhu BS, Wang XF, Lu QH, Chen WT, Zhou XJ (2008) Nanoscale surface topography enhances cell adhesion and gene expression of madine darby canine kidney cells. J Mater Sci Mater Med 19(5):2215–2222. https://doi.org/10.1007/s10856-007-3323-z
110. Zhu B et al (2004) Nanotopographical guidance of C6 glioma cell alignment and oriented growth. Biomaterials 25(18):4215–4223. https://doi.org/10.1016/j.biomaterials.2003.11.020
111. Ahmmed KMT, Montagut J, Kietzig AM (2017) Drag on superhydrophobic sharkskin inspired surface in a closed channel turbulent flow. Can J Chem Eng 95(10):1934–1942. https://doi.org/10.1002/cjce.22850
112. Rebollar E et al (2014) Physicochemical modifications accompanying UV laser induced surface structures on poly(ethylene terephthalate) and their effect on adhesion of mesenchymal cells. Phys Chem Chem Phys 16(33):17551–17559. https://doi.org/10.1039/c4cp02434f
113. Babaliari E et al (2018) Engineering cell adhesion and orientation via ultrafast laser fabricated microstructured substrates. Int J Mol Sci 19(7). https://doi.org/10.3390/ijms19072053
114. Schwibbert K, Menzel F, Epperlein N, Bonse J, Krüger J (2019) Bacterial adhesion on femtosecond laser-modified polyethylene. Materials (Basel) 12(19):16–25. https://doi.org/10.3390/ma12193107
115. Danilevicius P (2012) Micro-structured polymer scaffolds fabricated by direct laser writing for tissue engineering. J Biomed Opt 17(8):081405. https://doi.org/10.1117/1.jbo.17.8.081405

116. Cavalcanti-Adam EA, Aydin D, Hirschfeld-Warneken VC, Spatz JP (2008) Cell adhesion and response to synthetic nanopatterned environments by steering receptor clustering and spatial location. HFSP J 2(5):276–285. https://doi.org/10.2976/1.2976662
117. Xiong S, Gao HC, Qin L, Jia YG, Ren L (2019) Engineering topography: effects on corneal cell behavior and integration into corneal tissue engineering. Bioact Mater 4:293–302. https://doi.org/10.1016/j.bioactmat.2019.10.001
118. Ozan S, Lin J, Weng W, Zhang Y, Li Y, Wen C (2019) Effect of thermomechanical treatment on the mechanical and microstructural evolution of a β-type Ti-40.7Zr–24.8Nb alloy. Bioact Mater 4:303–311. https://doi.org/10.1016/j.bioactmat.2019.10.007
119. Biggs MJP, Richards RG, Gadegaard N, Wilkinson CDW, Dalby MJ (2007) The effects of nanoscale pits on primary human osteoblast adhesion formation and cellular spreading. J Mater Sci Mater Med 18(2):399–404. https://doi.org/10.1007/s10856-006-0705-6
120. Hao L et al (2018) Enhancing the mechanical performance of poly(ether ether ketone)/zinc oxide nanocomposites to provide promising biomaterials for trauma and orthopedic implants. RSC Adv 8(48):27304–27316. https://doi.org/10.1039/c8ra01736k
121. Kumar A, Yap WT, Foo SL, Lee TK (2018) Effects of sterilization cycles on PEEK for medical device application. Bioengineering 5(1). https://doi.org/10.3390/bioengineering5010018
122. Laurens P, Sadras B, Decobert F, Arefi-Khonsari F, Amouroux J (1998) Enhancement of the adhesive bonding properties of PEEK by excimer laser treatment. Int J Adhes Adhes 18(1):19–27. https://doi.org/10.1016/S0143-7496(97)00063-8
123. Wilson A, Jones I, Salamat-Zadeh F, Watts JF (2015) Laser surface modification of poly(etheretherketone) to enhance surface free energy, wettability and adhesion. Int J Adhes Adhes 62:69–77. https://doi.org/10.1016/j.ijadhadh.2015.06.005
124. Zheng Y, Xiong C, Wang Z, Li X, Zhang L (2015) A combination of CO 2 laser and plasma surface modification of poly(etheretherketone) to enhance osteoblast response. Appl Surf Sci 344:79–88. https://doi.org/10.1016/j.apsusc.2015.03.113
125. Nedela O, Slepicka P, Švorcík V (2017) Surface modification of polymer substrates for biomedical applications. Materials (Basel) 10(10). https://doi.org/10.3390/ma10101115
126. Vencl L, Ivanović L, Stojanović B, Zadorozhnaya E, Miladinović S, Svoboda P (2019) Surface Texturing for Tribological Applications: a Review. Proc Eng Sci 1(1):227–239. https://doi.org/10.24874/pes01.01.029
127. Henriques B et al (2018) Influence of laser structuring of PEEK, PEEK-GF30 and PEEK-CF30 surfaces on the shear bond strength to a resin cement. J Mech Behav Biomed Mater 84(May):225–234. https://doi.org/10.1016/j.jmbbm.2018.05.008
128. Liu M, Li MT, Xu S, Yang H, Sun HB (2020) Bioinspired superhydrophobic surfaces via laser-structuring. Front Chem 8(October):1–6. https://doi.org/10.3389/fchem.2020.00835
129. Cordero D, López-Álvarez M, Rodríguez-Valencia C, Serra J, Chiussi S, González P (2013) In vitro response of pre-osteoblastic cells to laser microgrooved PEEK. Biomed Mater 8(5). https://doi.org/10.1088/1748-6041/8/5/055006
130. Zheng Y, Liu L, Ma Y, Xiao L, Liu Y (2018) Enhanced osteoblasts responses to surface-sulfonated polyetheretherketone via a single-step ultraviolet-initiated graft polymerization. Ind Eng Chem Res 57(31):10403–10410. https://doi.org/10.1021/acs.iecr.8b02158
131. Michaljaničová I, Slepička P, Rimpelová S, Slepičková Kasálková N, Švorčík V (2016) Regular pattern formation on surface of aromatic polymers and its cytocompatibility. Appl Surf Sci 370:131–141. https://doi.org/10.1016/j.apsusc.2016.02.160
132. Pei X et al (2020) 3D printed titanium scaffolds with homogeneous diamond-like structures mimicking that of the osteocyte microenvironment and its bone regeneration study. Biofabrication 13(1). https://doi.org/10.1088/1758-5090/abc060